National Park Service
U.S. Department of the Interior

Natural Resource Stewardship and Science

Mapping of Erosion Features Related to Thaw of Permafrost in the NPS Arctic Inventory and Monitoring Network, Alaska

Natural Resource Technical Report NPS/ARCN/NRTR—2014/912

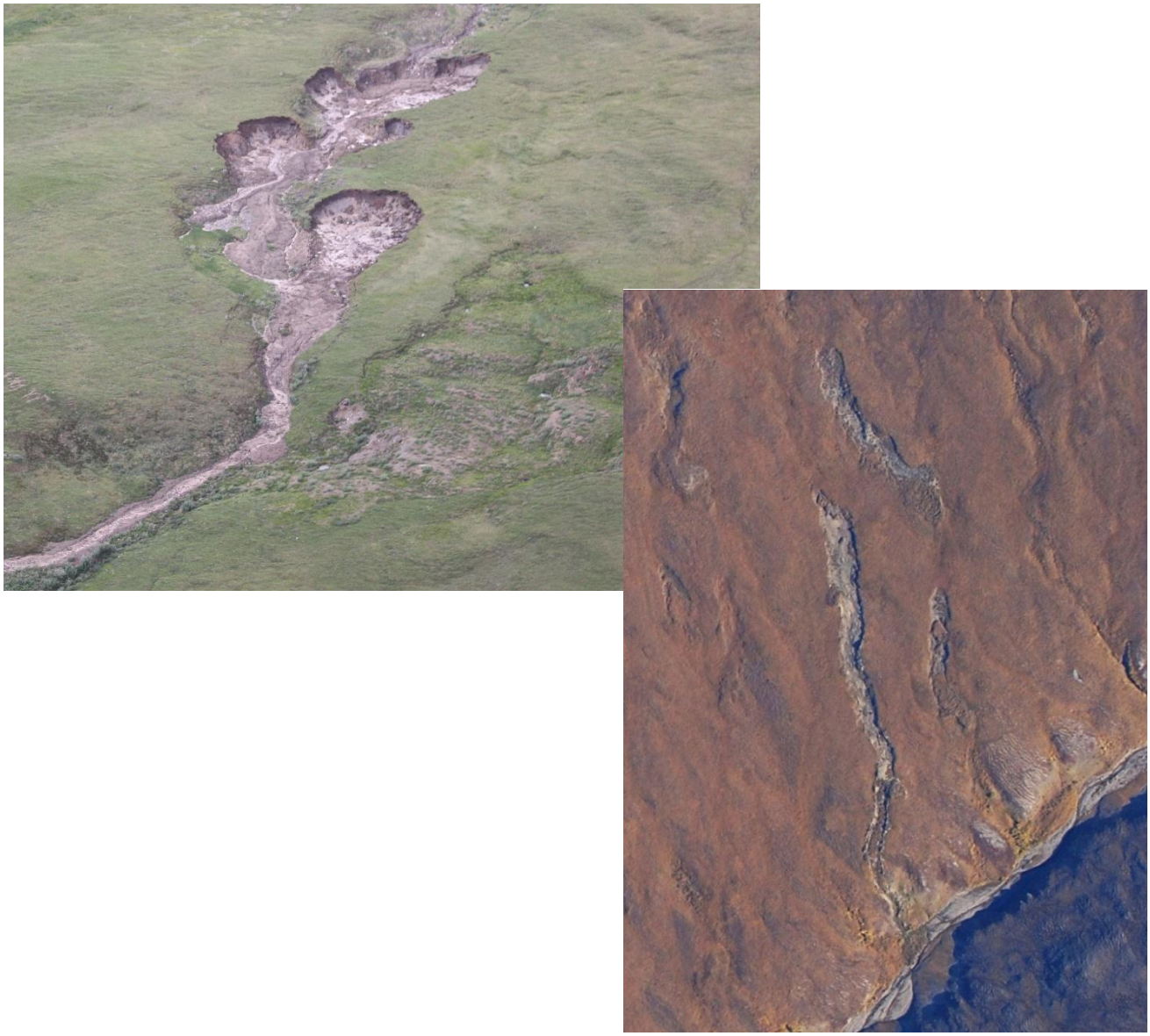

ON THE COVER

In the photo on the left, a cluster of several small retrogressive thaw slumps in Gates of the Arctic National Park and Preserve (longitude -154.186°, latitude 68.308°). The oval-shaped active slump in the center of the photo is about 15 m wide. A revegetated slump is visible below and to the right of the active slumps. In the photo on the right, three active-layer detachments (ALD) in the Noatak National Preserve (latitude 68.25°, longitude -157.90°). The grayish strips near the center of this photograph are bare soil exposed by downhill sliding of the vegetation and an approximately 1-m thick layer of thawed soil over permafrost. The largest ALD pictured is about 300 m long and 25 m wide. It ends near a small stream at the bottom of the photo. Photographs by: the author (left) and Tom George (right).

Mapping of Erosion Features Related to Thaw of Permafrost in the NPS Arctic Inventory and Monitoring Network, Alaska

Natural Resource Technical Report NPS/ARCN/NRTR—2014/912

David K Swanson

National Park Service
4175 Geist Rd
Fairbanks, AK 99709

October 2014

U.S. Department of the Interior
National Park Service
Natural Resource Stewardship and Science
Fort Collins, Colorado

The National Park Service, Natural Resource Stewardship and Science office in Fort Collins, Colorado, publishes a range of reports that address natural resource topics. These reports are of interest and applicability to a broad audience in the National Park Service and others in natural resource management, including scientists, conservation and environmental constituencies, and the public.

The Natural Resource Technical Report Series is used to disseminate results of scientific studies in the physical, biological, and social sciences for both the advancement of science and the achievement of the National Park Service mission. The series provides contributors with a forum for displaying comprehensive data that are often deleted from journals because of page limitations.

All manuscripts in the series receive the appropriate level of peer review to ensure that the information is scientifically credible, technically accurate, appropriately written for the intended audience, and designed and published in a professional manner.

This report received formal peer review by subject-matter experts who were not directly involved in the collection, analysis, or reporting of the data, and whose background and expertise put them on par technically and scientifically with the authors of the information.

Views, statements, findings, conclusions, recommendations, and data in this report do not necessarily reflect views and policies of the National Park Service, U.S. Department of the Interior. Mention of trade names or commercial products does not constitute endorsement or recommendation for use by the U.S. Government.

This report is available in digital format from the National Park Service, Arctic Inventory and Monitoring Network (http://science.nature.nps.gov/imn/units/arcn) and the Natural Resource Publications Management website (http://www.nature.nps.gov/publications/nrpm/). To receive this report in a format optimized for screen readers, please email irma@nps.gov.

Please cite this publication as:

Swanson, D. K. 2014. Mapping of erosion features related to thaw of permafrost in the NPS Arctic Inventory and Monitoring Network, Alaska. Natural Resource Technical Report NPS/ARCN/NRTR—2014/912. National Park Service, Fort Collins, Colorado.

NPS 953/126782, October 2014

Contents

Figures

Page

Tables

Page

Abstract

A map of active-layer detachments (ALD) and retrogressive thaw slumps (RTS) was completed for all of the National Park Service (NPS) Arctic Inventory and Monitoring Network (ARCN; the 5 NPS units in northern Alaska) using high-resolution satellite imagery from 2006 through 2009. ALD and RTS develop by localized thaw of permafrost and can expose significant areas of soil to erosion.

A total of 2246 ALD were identified in ARCN, mainly in the Noatak National Preserve (NOAT) and Gates of the Arctic National Park and Preserve (GAAR). The largest ALD covered just over 2 ha, and the total area of bare soil within ALD in ARCN was just under 300 ha. The mean surface slope for ALD polygons was 21%; 80% of all pixels mapped in ALD had slopes between 8% and 39%. ALD were most common on northwest- and west-facing slopes. ALD formed on a variety of surficial geologic materials, including solifluction deposits, glacial deposits, and loess. Vegetation in the vicinity of ALD included all the widespread upland tundra types, but did not include barrens (e.g. exposed rock or scree) or forest. Some of the ALD led to the formation of RTS. Most of the mapped ALD appear to have formed during the unusually warm summer of 2004. Since ALD are episodic and revegetate in 5-10 years, frequent re-sampling (at least every 5 years), or sampling triggered by evidence that an ALD event has occurred, will be required to monitor ALD.

A total of 724 RTS were identified in ARCN, nearly all of them in NOAT and GAAR. The total area of bare soil mapped in RTS was about 235 ha. The largest RTS covered about 9 ha in northwestern GAAR, but aside from this exceptional feature the largest RTS in ARCN were just over 4 ha. The mean slope of RTS as measured by GIS analysis was 17%, and 80% of all pixels in RTS had slopes between 4% and 30%. Most RTS were in late-Pleistocene glacial deposits. The vegetation in the vicinity of RTS was similar to ALD: it included all of the widespread upland tundra types, but not barrens or forest. RTS were most common on northwest-facing slopes and least common on south-facing slopes. Revegetated RTS were frequently observed in the vicinity of active RTS, and RTS are visible on historical aerial photographs from the 1950s and c. 1980. RTS grow for a decade or more, and could be mapped at 5- to 10-year intervals to determine trends in the area covered.

Glossary

Active layer. The surface layer of ground over permafrost that thaws and re-freezes annually.

Active-layer detachment (ALD). A mass movement feature consisting of active-layer material that slides on saturated fine-grained material over permafrost. ALD typically flow over a period of days to weeks in a single thaw season. An ALD exposes an area of bare soil and has a deformed mat of soil and vegetation at its lower end.

Colluvial. A general term for sedimentary slope deposits.

Georeference. To establish the map scale and location of an image, such as an aerial photograph. Simple georeferencing of an aerial photograph typically uses an affine transformation to approximately scale and locate the photograph in real-world coordinates, but it does not correct for distortions due to topography and the camera lens.

Glacial drift. Sediment deposited by glaciers or by flowing water derived from glaciers and in their immediate vicinity.

Glacial till. Sediment deposited by glaciers.

Glaciolacustrine. Sediments deposited in glacial lakes (lakes bordered at least in part by glaciers).

Granitic. Rock that crystallized from a melt and is rich in silicon.

Ground ice. Ice contained in frozen ground, including massive ice bodies such as ice wedges, and ice in small pores or cavities.

Ice segregation. The process by which ground ice accumulates in discrete layers by movement of water through soil pores and subsequent freezing.

Ice wedge. A generally wedge-shaped body of ice present in permafrost and produced by contraction cracking followed by infilling and freezing of water.

IKONOS. An earth observation satellite that gathered multispectral imagery with a pixel size (resolution) of 4 m and panchromatic imagery with a pixel size of 1 m.

Loess. Wind-deposited, silty sediment.

Metasedimentary rock. Sedimentary rock that has been subject to heat and pressure sufficient to alter its mineralogy and physical properties.

Multispectral. An image containing two or more wavelength bands across the spectrum.

Normalized Difference Vegetation Index (NDVI). A numerical index computed from multispectral imagery by the following formula: NDVI = (NIR - R)/NIR + R), where NIR is a near-infrared (0.757 to 0.853 µm on IKONOS images) reflectance measurement and R is a red (0.632 to 0.698 µm on

IKONOS images) reflectance measurement. NDVI is an indicator of the greenness of vegetation and can be used to estimate biomass.

Orthorectification. The process by which an aerial photograph is corrected for distortions due to perspective, the camera, and terrain to produce an image with map coordinates and a consistent scale.

Panchromatic. Image that contains one wavelength band corresponding to a sum of all visible wavelengths.

Permafrost. Ground that remains at or below the 0°C for 2 or more consecutive years. Most permafrost in ARCN has been frozen for many years, even thousands of years. Permafrost may be present in materials that contain considerable ice, or materials such as bedrock with very little ice.

Pleistocene. The geologic epoch lasting from approximately 2,588,000 to 11,700 years ago. The Pleistocene was a time of repeated earth glaciations.

Raster. A matrix of cells (known as pixels) arrayed in rows and columns, where each cell contains data, such as color in a satellite image.

Retrogressive thaw slump (RTS). A mass movement caused by thaw of permafrost, consisting of an escarpment that advances upslope as material thaws and is transported away by viscous flow and water erosion.

Sedimentary rock. Rock derived from particles or precipitates deposited in water or air. Includes *clastic* rocks (such as sandstone or siltstone, derived from particles) and *carbonate* rocks (such as limestone) dominated by calcium and magnesium carbonate minerals.

Solifluction. The downslope flow of wet, unfrozen material over frozen material. Refers to a slower process than that which produces active-layer detachments. The vegetation and organic soil surface mat on soliflucting material typically remains intact.

Thaw degree-day. An index of the heat available for thaw. The difference between the daily mean temperature and 0° C is computed for each day and summed over a period of days, such a single thaw season.

Thermokarst. Subsidence of the ground surface due to thaw of ice in permafrost.

Tundra. Treeless vegetation of arctic and alpine regions.

Ultramafic. A class of igneous rocks (rocks solidified from a melt) very rich in magnesium and iron.

Volcanic rock. Rock that originated from the eruption of a volcano, such as basalt, andesite, or rhyolite.

Yedoma. Very ice-rich permafrost material consisting of organic-rich loess with large bodies of massive ice of ice wedge origin, formed in unglaciated areas during cold periods of the Pleistocene.

Introduction

Permafrost thaw can lead to subsidence of the ground surface, mass movement of material on slopes, and exposure of bare soil to erosion by water. While localized thaw and refreezing of permafrost occurs under a stable cold arctic climate, climate change has been cited as a cause of recent increased thaw of permafrost in Alaska (Jorgenson et al. 2006). Concerns about the state of permafrost in the future led the National Park Service Arctic Inventory and Monitoring Network (ARCN, Fig. 1), to include permafrost as a monitoring "Vital Sign" (Lawler et al. 2009). Thaw-related slumping and associated soil erosion may have increased in ARCN in recent years (Balser et al. 2007), and an important component of ARCN's permafrost vital sign monitoring involves locating and mapping subsidence and erosion features related to permafrost thaw.

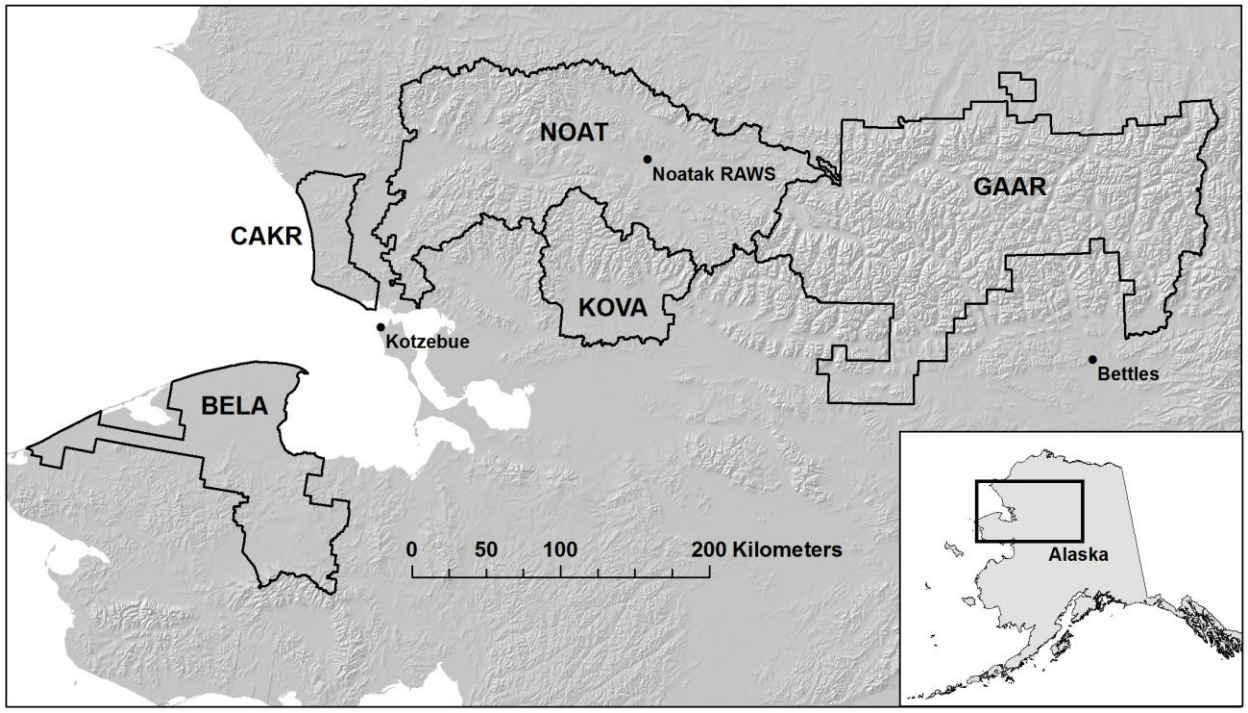

Figure 1. The NPS Arctic Inventory and Monitoring Network (ARCN). The NPS units in ARCN are the Bering Land Bridge National Preserve (BELA), Cape Krusenstern National Monument (CAKR), Gates of the Arctic National Park and Preserve (GAAR), Kobuk Valley National Park (KOVA), and the Noatak National Preserve (NOAT).

Two important erosion features related to permafrost thaw in ARCN are active-layer detachments (ALD) and retrogressive thaw slumps (RTS; Balser et al. 2010, Swanson and Hill 2010, Swanson 2012a,b, Swanson 2013). ALD are small landslides that occur on vegetated slopes (Fig. 2). A surface layer roughly 1 m thick slides as a unit held together by the root mat, and accumulates on the footslope. ALD are typically 10 to 30 m wide and from tens to several hundred meters long. The slide leaves an elongated region of bare soil exposed on a slope, which can lead to erosion of sediment into streams (Bowden et al. 2008, Lamoureux and Lafrenière 2009). ALD tend to occur in clusters, where soil and slope conditions are favorable, after periods of unusually warm summer weather and possibly also high rainfall (Carter and Galloway, 1981; Lewkowicz and Harris 2005).

They probably occur after thaw of the ice-rich layer, known as the "transition zone" (Shur et al. 2005), which is often present in the upper permafrost. This produces a mud slurry that lubricates the downslope flow of an elongate strip of cohesive surface soil over frozen ground (Lewkowicz and Harris 2005, Lewkowicz 2007). RTS occur where a cut-bank in ice-rich permafrost advances into undisturbed ground as material thaws in the steep bank, falls or slumps onto the adjacent more gentle slope, and then is transported away by water erosion, sliding, or viscous flow (Burn and Lewkowicz 1990; Fig. 3). RTS are deeper than ALD: the eroding cut-bank is typically 2- to 10-m high. RTS often begin as an escarpment produced by marine, lakeshore, or riverbank erosion, or by an ALD. As they advance by thawing and slumping, they can shed large amounts of sediment into the adjacent water body and affect water chemistry (Crosby 2009, Kokelj et al. 2005, Bowden et al. 2012). Very ice-rich material of substantial thickness (e.g., several meters) and lateral extent is needed to produce a RTS (Fig. 4).

Figure 2. Active-layer detachments (ALD) in the Noatak National Preserve (latitude 68.25°, longitude -157.90°). The grayish strips near the center of this photograph are bare soil exposed by downhill sliding of the vegetation and an approximately 1-m thick layer of thawed soil over permafrost. The largest ALD pictured is about 300 m long and 25 m wide. It ends near a small stream at the bottom of the photo.

The newly acquired, nearly complete coverage of ARCN by high-resolution satellite images has allowed the NPS to make a comprehensive survey of erosion features caused by permafrost thaw. I combined automated mapping methods with visual recognition of these geomorphic features to make a comprehensive map of ALD and RTS. Mapping in four of the ARCN NPS units was reported previously: Bering Land Bridge National Preserve (BELA), Cape Krusenstern National Monument (CAKR) and Kobuk Valley National Park (KOVA)(Swanson 2010), and the Noatak National Preserve (NOAT; Swanson 2012b). Mapping is now complete for the final ARCN NPS unit, Gates of the Arctic National Park and Preserve (GAAR). The present report compiles the new data from GAAR with the previous data into an ARCN-wide summary of the occurrence of ALD and RTS, and their relationships with environmental factors (topography, vegetation, and surficial geology).

Figure 3. A cluster of several small retrogressive thaw slumps in GAAR. The oval-shaped active slump in the center of the photo is about 15 m wide. A revegetated slump is visible below and to the right of the active slumps. Photo date 15 July 2010, longitude -154.186°, latitude 68.308°.

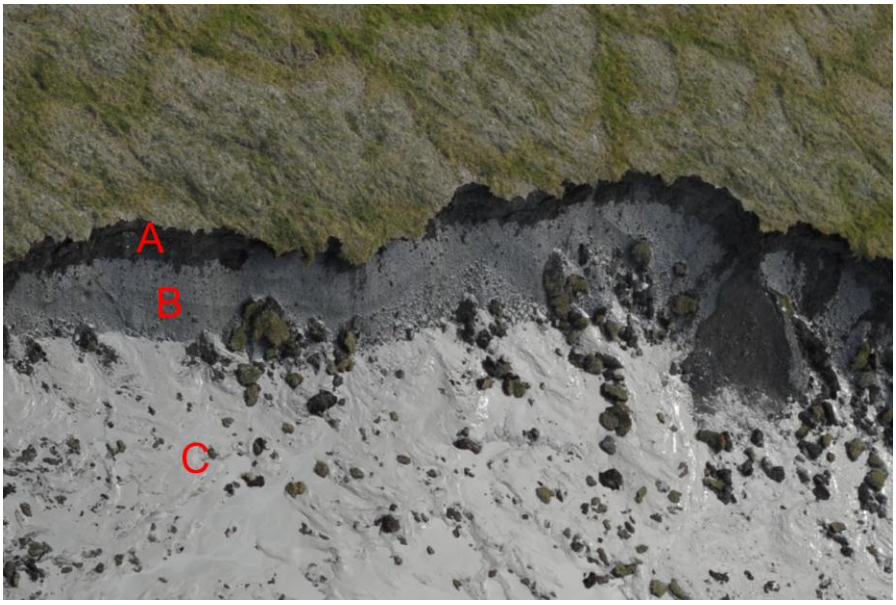

Figure 4. Oblique aerial photograph of the escarpment in a RTS in NOAT. The scarp is 4-5 m high and exposes glacial till forming a vertical face (A) over sloping, debris-rich glacial ice with foliation visible (B), leading down to a zone of liquefied mud produced by thaw (C). Slump NOAT0070 on 19 July 2011, near longitude -156.82°, latitude 67.96°.

Methods

Study Area

This study covers all of ARCN, the 5 NPS units in northern Alaska (Fig. 1). Permafrost is continuous (permafrost covers 90% or more of the landscape) across most of ARCN, with only the very southern part of KOVA in the discontinuous permafrost zone (50-90% of the landscape with permafrost; Jorgenson et al. 2008). Ground ice content is moderate (10-40% by volume) to high (more than 40% by volume) in unconsolidated sediments of lowlands and mountain valleys throughout the study area, and low in bedrock-cored highlands (Jorgenson et al. 2008). The mean annual air temperature is -8.2°C (January mean -26.1°C, July 13.1°C) at the Noatak Remote Alaska Weather Station (RAWS; Fig. 1); this station has nearly continuous records since 1990 and is centrally located with respect to much of ARCN. The 1981-2010 mean annual air temperature at Kotzebue Airport National Weather Service station (NWS), which is representative of the more maritime areas of ARCN, was -5.1°C (January: -19.3°C, July: 12.5°C).

Much of ARCN is mountainous (Fig. 5). In GAAR the mountains are rugged with flat-bottomed, U-shaped valleys. NOAT is ringed by rugged mountains, with the central portions occupied by more rounded mountains and gently sloping lowlands. KOVA has rugged mountains in the north and plains or low hills in the south. The northern part of BELA and the coastal parts of CAKR are occupied by nearly flat coastal plains, while the remainder of these parks are predominantly rounded low mountains, hills, or gently sloping lowlands.

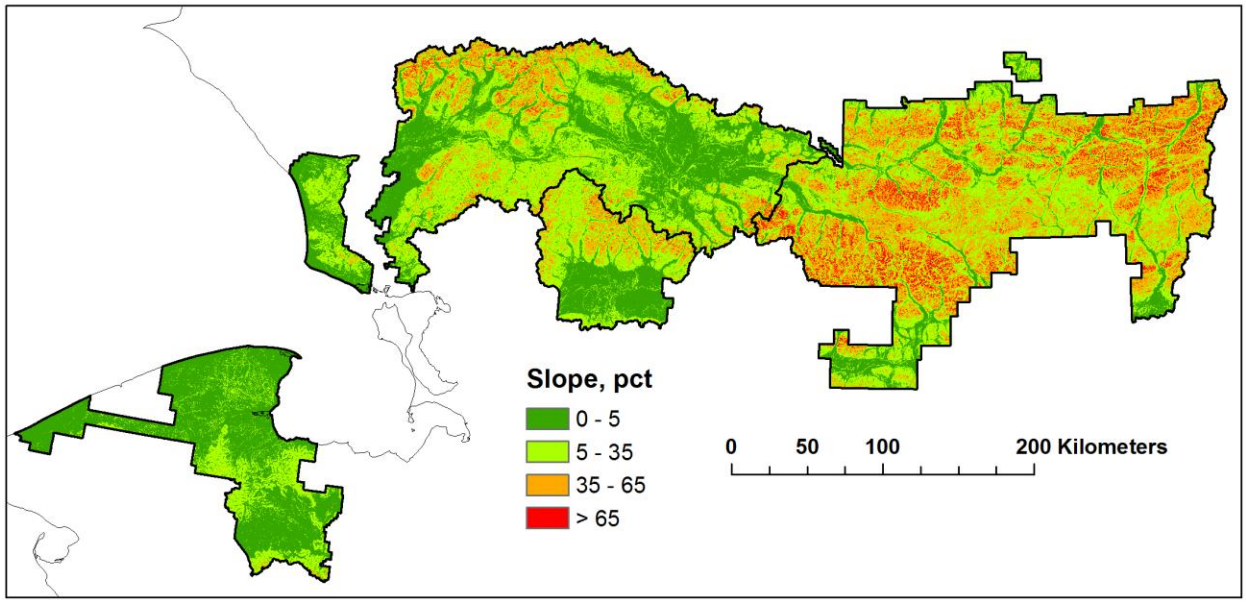

Figure 5. Slope steepness in ARCN. Slopes of 0 to 5% are nearly flat. Slopes of 5-35% are gentle to moderate and in the optimal range for both ALD and RTS erosion features (see the Results section). Slopes greater than 35% are steep and occur mainly in rugged mountains; slopes greater than 65% are mostly exposed rock.

Most of GAAR and NOAT were glaciated during the late Pleistocene; lower mountain slopes and valley bottoms there are covered by glacial or glaciolacustrine deposits (Hamilton 2010, Hamilton

and Labay 2011). Steeper slopes and ridges have exposed bedrock or coarse-grained slope deposits derived from both glacial till and adjacent bedrock. Most of CAKR and BELA were not glaciated in the Pleistocene (Hopkins 1963, Péwé 1975). The plains in northern BELA include some areas of "yedoma" terrain, which consists of tens of meters of organic-rich loess (silty, wind-deposited sediments) with large ice wedges that formed in unglaciated areas during Pleistocene glacial times (Kanevskiy et al 2011). Thinner loess (a meter or two) with large ice wedges occurs locally on top of glacial till in NOAT (Swanson and Hill 2010). This is older glacial till that was deposited prior to the last glacial maximum (LGM) and then was exposed during the LGM, when the loess and ice-wedges formed.

The bedrock exposed in mountainous areas over most of ARCN consists of mainly of sedimentary rocks or metasedimentary rocks (Mayfield et al. 1983, Moore et al. 1994). Volcanic rocks are present in the lowlands of BELA, and minor areas of granite occur in GAAR.

The vegetation of ARCN consists mainly of arctic tundra, with spruce and birch forest at low elevations in the southern part of the interior parks (Fig. 6).

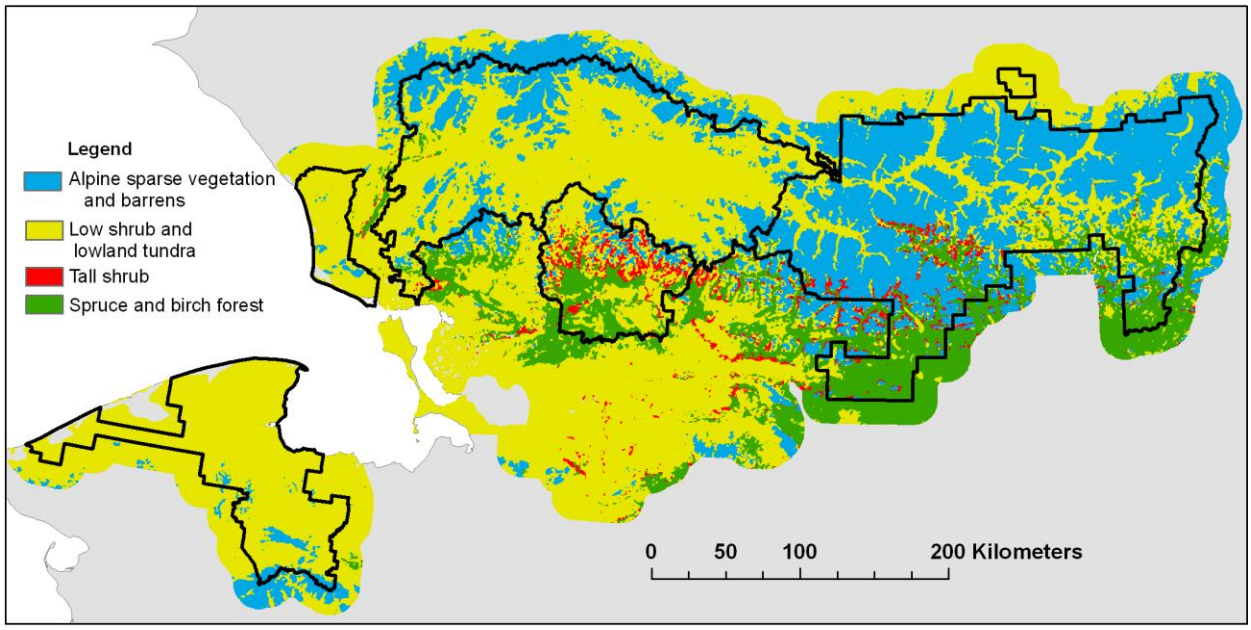

Figure 6. Generalized vegetation of ARCN (from Jorgenson et al. 2009).

Mapping Methods

Exposed bare soil areas originating from ALD and RTS were mapped by a partially automated method involving both machine processing and visual interpretation of high-resolution imagery The automated process utilized the unique spectral properties of exposed bare soil areas surrounded by vegetation to rapidly delineate unvegetated areas, while visual interpretation was used to take advantage of the human eye's ability to rapidly and accurately differentiate ALD and RTS from other areas of exposed bare soil, such as river gravel bars or mountain ridge tops.

Exposed bare soil was mapped here rather than the total area affected by the ALD or RTS. Thus the boundaries of ALD and RTS generally exclude large mats or rafts of vegetation that survived transport, and formerly bare areas that were in various stages of revegetation at the time of the image. This convention was adopted because transported mats and revegetated areas are difficult to separate from undisturbed vegetation by automated means, and because the bare soil represents the area of greatest impact.

IKONOS multispectral satellite imagery (http://www.geoeye.com) was used for mapping. This imagery includes blue, green, red and near-infrared spectral bands with 4 m resolution, pan-sharpened to 1 m resolution. The images examined were from the snow-free period (late June through early October) of 2006 through 2009. Images were orthorectified with the best available ARCN-wide digital elevation model, the National Elevation Dataset at 60 m resolution (USGS, 2006), and projected to the Alaska Albers projection.

Clouds obscured portions of the study area on the imagery. While erosion features could occasionally be located in gaps between the clouds, mapping is incomplete in these areas. Cloudy areas are depicted on the maps in the Results section.

Erosion features were mapped by a 3-step process: 1) digitize bare-soil polygons by automated process, 2) manually create a point layer marking all ALD and RTS visible on imagery, with the feature type as an attribute, and 3) join these two layers to extract permafrost-related bare soils areas and eliminate non-target bare soil areas (such as river gravel bars and bedrock exposed on mountain ridges), and transfer the erosion-feature type information to the polygons (Fig. 7). Further details of the mapping process are given below.

Delineation of bare-soil polygons

The normalized difference vegetation index (NDVI) was computed from the near infrared (NIR) and red spectral bands of the IKONOS images. NDVI is a measure of "greenness" that is closely related to leaf area and biomass (Tucker and Sellers, 1986). NDVI is (NIR - red)/(NIR + red). It is high (near 1) in densely vegetated areas and zero or lower in unvegetated areas. A median filter using a circle with a radius of 3 pixels was applied to the NDVI image, to reduce speckling in the images while preserving features greater than 10 m across. (The median filter passed a window across the NDVI image, at each position computed the median value of all pixels within the circle, and assigned the median to the center pixel.) Next, a threshold NDVI value was chosen for each image to best separate vegetated and unvegetated areas; this value was usually between 0 and -0.1. In practice, this threshold value was chosen during the next step, visual identification of erosion features. Finally, the unvegetated areas (with NDVI below the threshold) were converted from raster (pixel) format to polygons.

Identification of permafrost thaw-related erosion features

The point layer of permafrost-related erosion features (ALD and RTS) was produced by systematic examination of the images. Images were displayed in the color scheme of color-infrared aerial photographs to enhance visibility of unvegetated areas. A grid with 4- by 4-km cells was placed over each image, and each cell in the grid was searched at 1:20,000 scale for any potential ALD or RTS,

which were then examined at a larger scale (1:5,000 or larger) to verify and label them as ALD or RTS. The NDVI image was turned on and off over the color-infra-red image to help locate bare-soil areas and determine the appropriate NDVI threshold value to use for mapping bare-soil areas in each particular satellite image as described above. Features with 2 or more separate patches of bare soil that were part of a single feature (e.g., an ALD with a block of vegetation that slid partway down and separated the bare soil into two patches) were given multiple points with the same identifying code.

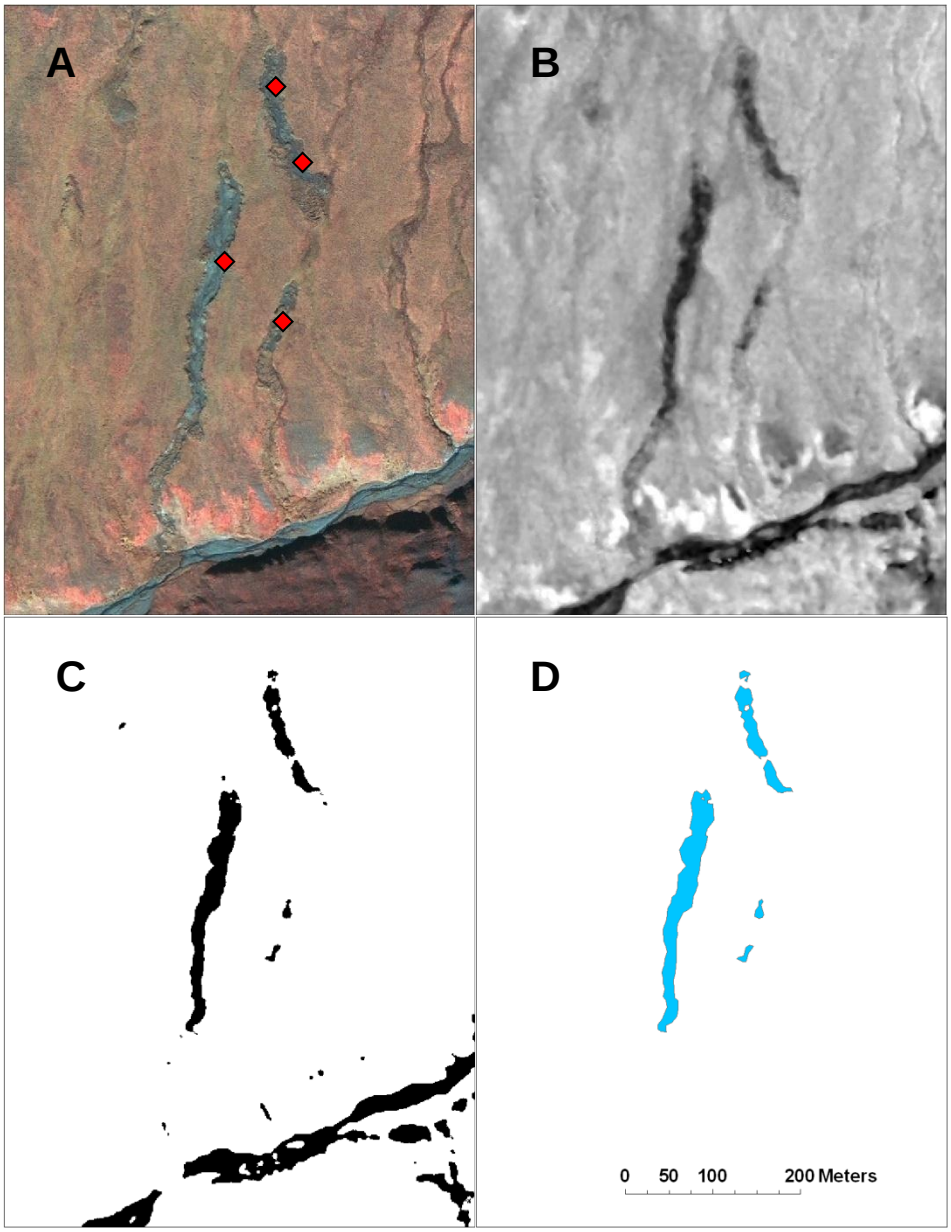

Figure 7. Method for mapping of the erosion features due to thaw of permafrost. A) IKONOS image with color-infrared color scheme and ALD marked with points. B) NDVI of the IKONOS image. C) NDVI image thresholded to differentiate bare earth (black) from vegetated areas (white). D) Polygons produced by conversion of the thresholded image to a polygon layer and intersection with points in (A). These are the ALD depicted in Fig. 2, near latitude 68.25°, longitude -157.90°.)

ALD leave strips of bare soil 10 to 30 m wide and up to hundreds of meters long on slopes; they stand in sharp contrast to adjacent, densely vegetated areas. ALD are distinguished from other bare soil areas by their shape, the presence of a deformed soil-vegetation mat at their downhill end, and their orientation perpendicular to the slope. Features that are possibly confused with ALD include: 1) elongated snow beds. which lack the deformed vegetation-soil mat, are often oriented across the slope, and often have a snow patch in summer images; 2) elongated eroded areas along small streams, which also lack the deformed vegetation mat, typically have pointed as opposed to blunt ends, and have a stream entering and exiting from their upper and lower ends; and 3) elongated patches of scree or rubble, which again lack the deformed vegetation-soil mat and typically occur in a pattern related to bedrock outcrops.

The features of RTS that distinguish them from other unvegetated areas include: 1) generally round shape with an escarpment visible as a shadow along part of the perimeter; 2) location on slopes with fine-grained geologic materials, as opposed to terrain with coarse rubble or exposed bedrock; and 3) evidence for of significant sediment transport from the RTS, in the form of a debris fan and sediment-laden water (Lacelle et al., 2010). Many RTS occur along a river or lakeshore bluff that provided the initial exposure of permafrost to thaw.

Spatial join of polygon and point layers

Bare-soil polygons that either contained a thaw-feature point within them, or had a point fall within 20 m of their boundaries were identified by automated process and given the attributes of the point. All other bare-soil polygons were deleted. This spatial join eliminated the numerous bare polygons of other origins, such as river gravel bars and bedrock outcrops. The resulting polygons were inspected and edited as needed, most often to remove unwanted areas (e.g., a river gravel bar that was contiguous with a slump and was joined with it into one polygon.) The area of each ALD or RTS was then computed; as mentioned previously, these areas do not include the displaced vegetated mats typically present at the lower end of an ALD, or portions of ALD or RTS that had been recolonized by vegetation.

Analysis of Environmental Factors

The count and area of ALD and RTS were summed for NPS administrative units and major watersheds: level 8 watersheds of the National Hydrography Dataset (USGS 2014). The proportion of the level 8 watersheds covered by ALD and RTS was computed and expressed in units of percent times 10^4, which is equivalent to proportion of area times 10^6, i.e. parts per million (ppm) of area. The relationship of erosion features to surficial geology was determined by overlay of feature center points onto the surficial geologic maps of GAAR and NOAT (Hamilton 2010, Hamilton and Labay 2011).

The relationship of the erosion features to topographic slope and aspect were determined by overlay of the erosion feature polygons (e.g., Fig. 7D) onto slope and aspect raster maps. The slope and aspect rasters were derived by the NPS Alaska Regional Office from the 60 m National Elevation Dataset (NED) digital elevation model (DEM); the 60 m NED DEM raster was re-sampled to 30 m using cubic convolution (i.e., it was smoothed) before computation of slope and aspect. The resolution of the erosion feature layer (derived from IKONOS images with 1 m resolution) is much

finer than the NED DEM (30 m). As a result of the coarseness of the DEM, the slopes and aspects associated with any given erosion feature include data derived from an area up to several tens of meters outside of the feature's boundaries, which probably increases variability but should have minor effects on the mean slope and aspect associated with ALD or RTS. The slope and aspect of all pixels within the erosion features were used to compute summary statistics; thus each feature influenced the resulting statistics in proportion to its size.

The vegetation of the erosion features was determined by overlay of the erosion features on the map of ecotypes (composite land cover-vegetation-soil mappings units) by Jorgenson et al. (2009). As in the case of the topographic rasters, the ecotype raster had coarser resolution (30 m) than the erosion feature maps (1 m) and thus the ecotypes were influenced by a neighborhood up to a few tens of meters outside the erosion feature boundaries. In principle, our erosion features should be mapped as one of the "barrens" ecotypes, but in practice they were not, because most were not present on the 2002 satellite imagery used in the ecotype mapping, and those that were present in 2002 were small enough at that time to have little effect on the 30 m pixels used for ecotype mapping. So in effect, overlay of the erosion feature footprints onto the ecotype maps gives the vegetation of the erosion feature footprints and their immediate vicinity just prior to their formation.

A simple map of expected ALD density in ARCN was created as follows. Areas with unsuitable ecotypes for ALD occurrence (see the Results and Discussion section below) were masked using the ecotype map of Jorgenson et al. (2009). Next the area covered by slope steepness classes 0-5%, 5-10%, 10-15%, etc. was computed for all of ARCN and for ALD alone was computed. The ratio between the area of ALD and the area in all of ARCN for each slope steepness class was computed. This ratio was used to reclassify the ARCN slope steepness raster into units of expected ALD area per unit land area.

Results and Discussion

Active-layer Detachments

ALD Overview

A total of 2246 ALD were identified in ARCN, and most were in NOAT and GAAR (Table 1, Fig. 8). The total area of bare soil in ALD was just under 300 ha. The ALD ranged in area from approximately 2 ha for large features to a few square meters for small or nearly revegetated features. An example of a large ALD is shown in Fig. 9. The Noatak River watershed in NOAT and GAAR contained the most ALD (Table 2). However, when the area covered by ALD was computed as a proportion of the watershed, the density of ALD in the Killik River watershed (GAAR) was similar to the density of ALD in the Noatak, and the density in the Nigu-Etivluk watersheds (in northeastern NOAT and northwestern GAAR) was greater (Table 2).

Table 1. Count and total area covered by ALD and RTS in ARCN

	ALD		RTS	
NPS unit	**Count**	**Area, ha**	**Count**	**Area, ha**
BELA	22	2.9	0	0
CAKR	22	1.7	0	0
GAAR	1324	179.9	429	136.0
KOVA	15	1.6	3	0.4
NOAT	863	109.7	292	99.2
ARCN (total)	2246	295.8	724	235.6

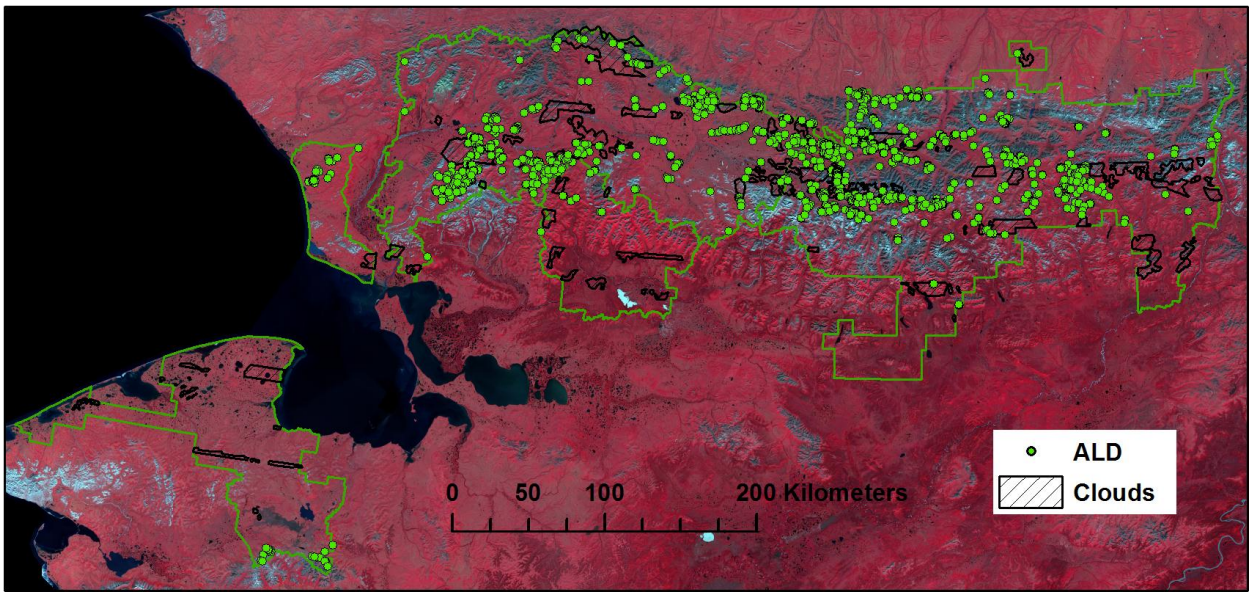

Figure 8. Active-layer detachments (ALD) in ARCN. Areas outlined as “clouds” were obscured on the imagery, and mapping in these areas is incomplete.

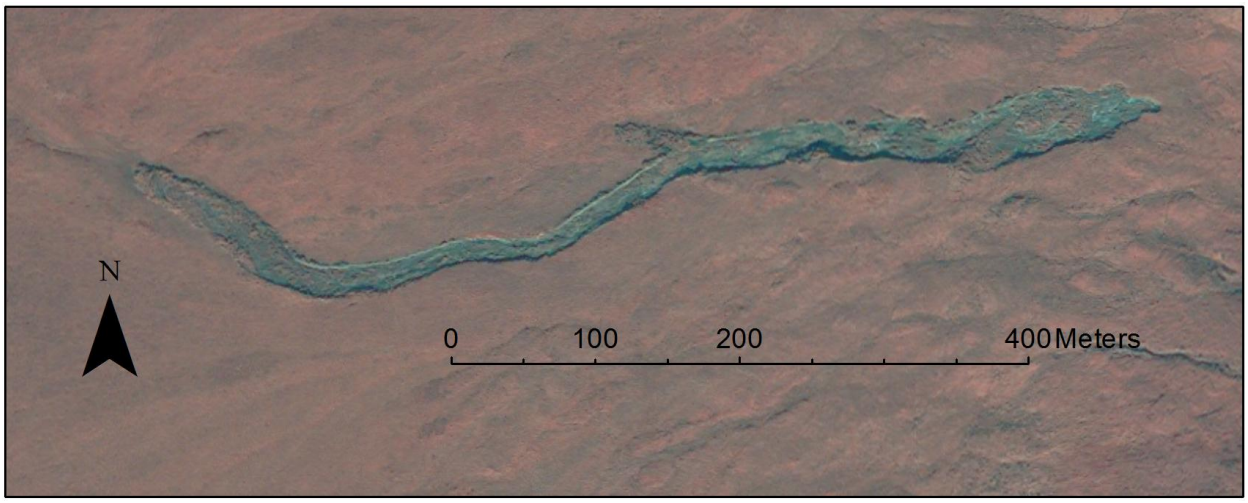

Figure 9. A large active-layer detachment. This ALD was about 750 m long and exposed about 1.5 ha of bare soil. It was located near the source of the Nigu River in northwestern GAAR (feature GAAR1341, longitude -155.04327°, latitude 67.9904°). The slope is from right to left, and an accumulation of slide material is visible at the lower (left) end of the ALD.

Table 2. Count and total area of ALD and RTS by watershed

		ALD			RTS		
Watershed	**Area[1], km^2**	**Count**	**Area, ha**	**Area[2], %X10^4**	**Count**	**Area, ha**	**Area[2], %X10^4**
Alatna River (GAAR)	4439	148	13.8	31	42	10.8	24
Chandler-Anaktuvuk Rivers (GAAR)	2658	6	0.2	1	16	5.9	22
Imuruk Basin (BELA)	1932	13	2.1	11	0	0	0
Killik River (GAAR)	5427	153	30.9	57	41	9.7	18
Middle Kobuk River (KOVA)	7431	15	1.6	2	3	0.4	1
Upper Kobuk River (GAAR)	4579	7	0.6	1	0	0	0
Koyukuk River (GAAR)	10516	199	23.5	22	172	33.3	32
Noatak River (GAAR-NOAT)	31253	1364	177.3	57	425	155	50
Norton Bay (BELA)	368	9	0.8	22	0	0	0
Nigu-Etivluk Rivers (GAAR, NOAT)	1156	310	42.7	369	25	20.5	177
Wulik-Kivalina Rivers (BELA)	1678	22	1.7	10	0	0	0

[1]Areas were measured for the portion of the watershed within the NPS unit

[2]"Area, %X10^4" is the total area covered by ALD or RTS as a fraction of the watershed area in percent times 10^4, which is the same as times areal fraction times 10^6, i.e parts per million of area.

ALD and Environmental Factors

The median surface slope for ALD polygons measured by GIS analysis was 18% and the mean was 21%. Two thirds of all pixels in ALD had slopes between 10% and 33%, 80% were between 8% and 39% slope, 90% were between 6 and 44% slope (Fig. 10). Presumably, very gentle slopes do not provide sufficient shear stress to trigger ALD movement, while steeper slopes tend to be bedrock, or

coarse-grained materials lacking sufficient ground ice. ALD were most common on northwest-facing slopes and least common on southeast-, and east-facing slopes (Fig. 11).

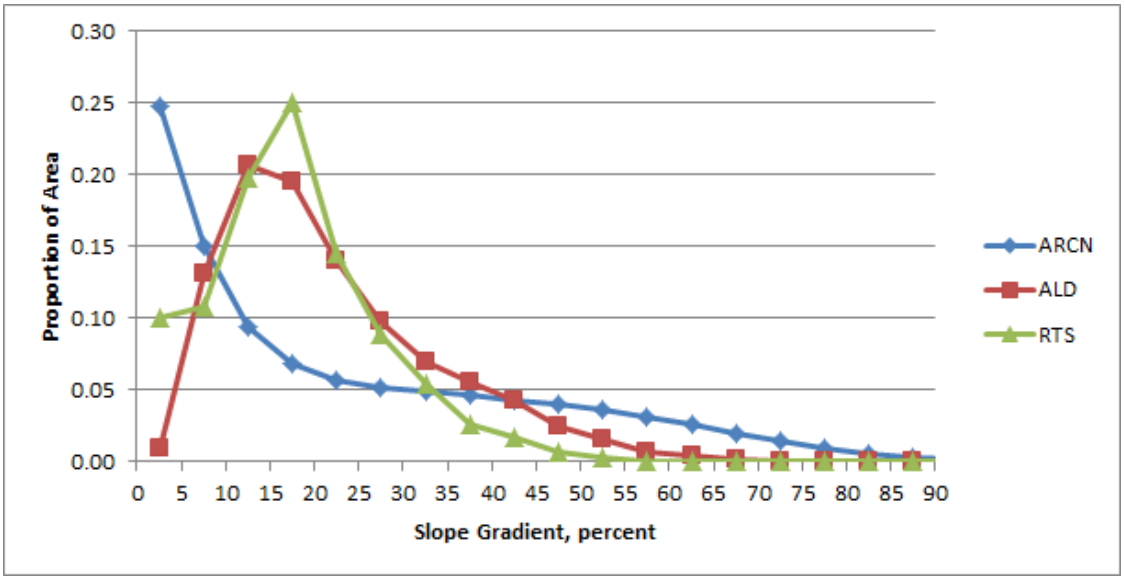

Figure 10. Slopes steepness of ALD and RTS. The markers give the proportion of area with slopes in "bins" 5% wide. For example, about 0.25 of the RTS area had slope steepness between 15% and 20%. The "ARCN" curve shows the distribution of slope steepness across all of ARCN.

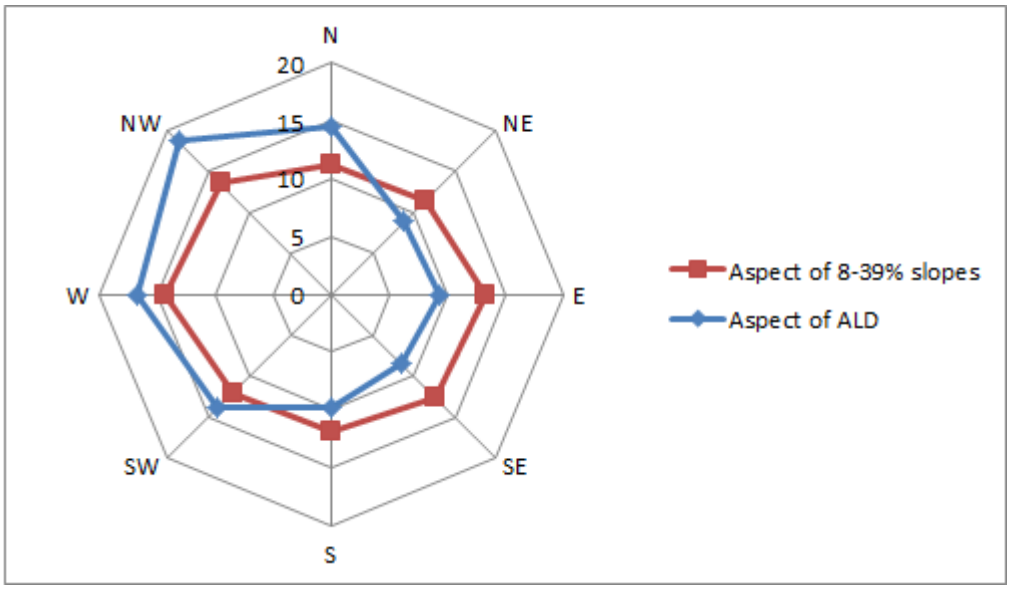

Figure 11. Slope aspects of ALD. "Aspect of ALD" is the percentage of all bare-soil pixels in ALD with the indicated aspect. For example, 18.5% of the ALD area had northwest aspects (between 292° and 238°). The red line is the proportion of each aspect in ARCN on slopes where steepness is in the optimal range for RTS (8 to 39% slope).

The most common surficial geologic unit obtained by overlay of ALD locations onto surficial geologic maps by Hamilton (2010) and Hamilton and Labay (2011) was "bedrock", though none of the features I mapped were on exposed rock per se. At the scale of the surficial geologic maps

(1:300,000) “bedrock” units include thin colluvial deposits and glacial till overlying bedrock in a mosaic with bedrock outcrops, and the ALD actually occurred on the surficial sediments. The most common of the actual surficial deposits mapped by Hamilton(2010) and Hamilton and Labay (2011) in locations with ALD were solifluction deposits, thin loess (windblown silt) over bedrock, and glacial drift from the Itkillik glaciation.

The association of ALD with bedrock lithology is difficult to analyze, because of the lack of a comprehensive geologic map of the study area, and the fact that ALD occur on surficial sediments, not bedrock. Clastic sedimentary and metasedimentary rocks dominate the mountains of NOAT and GAAR (Mayfield et al. 1983, Moore et al. 1994), and the bulk of ALD occur on slopes below these lithologies. Fewer are located in the vicinity of the carbonate, ultramafic, and granitic bedrock exposures that occur in parts of NOAT and GAAR, though whether this represents coincidence or some bedrock control on ALD formation is unknown. Bedrock lithology may play an indirect role in governing ALD formation through weathering: fine-grained clastic sedimentary rocks weather to silty surficial sediments that are more susceptible (than coarse-grained sediments) to ice segregation and thus ALD formation. However, ALD occur in the surficial sediment mantle that can be derived from distant (glacial, eolian) sources in addition to local weathering.

The vegetation in the vicinity of ALD includes all of the widespread upland tundra types (Table 3). ALD were nearly absent on alpine barrens ecotypes and all coastal, lowland, riverine, and forested ecotypes.

Table 3. Vegetation Near Active-Layer Detachments

Ecotype[1]	Percentage of ALD area in ecotype[2]	Percentage of ARCN occupied by ecotype
Upland Dwarf Birch-Tussock Shrub	28.6	20.1
Upland Birch-Ericaceous-Willow Low Shrub	23.2	11.3
Alpine Dryas Dwarf Shrub	20.3	14.3
Upland Alder-Willow Tall Shrub	8.3	4.9
Upland Sedge-Dryas Meadow	8.1	6.0
Alpine Ericaceous Dwarf Shrub	5.1	2.0

[1]Ecotypes are composite soil-vegetation units mapped by classification of 2002 Landsat satellite imagery (30 m resolution) by Jorgenson et al. (2008).

[2]These proportions reflect vegetation in and within a few tens of meters of the mapped ALD outlines (as a result of the 30 m resolution of the ecotype map), prior to their formation (because most were probably not present in 2002). The table includes all types that make up 5% or more of the overall ALD area; together these 6 ecotypes account for 94% of the area in ALD.

ALD in this study were found only in tundra environments, but I have observed multiple ALD that formed after a fire in a forested area of Yukon-Charley Rivers National Preserve (for example, near longitude -143.163°, latitude 65.333°; the ALD were visible on 2006 aerial photos after a 2004 wildfire). ALD in the taiga zone in Canada observed by Lewkowicz and Harris (2005), Lipovsky et al. (2005), and Lipovsky and Huscroft (2006) were also triggered by wildfires. Thus it is possible that wildfires could trigger ALD on forested slopes of KOVA and GAAR in the future.

The map of expected area of ALD in ARCN, derived from the slope and vegetation of ALD (see the Methods section), is compared with ALD locations in Fig. 12. ALD were common on favorable terrain as defined by slope and ecotype, and essentially absent on unsuitable terrain, such as the lowlands in northern BELA and eastern NOAT (which are too flat), or the largely barren, rugged mountains of northeastern GAAR.

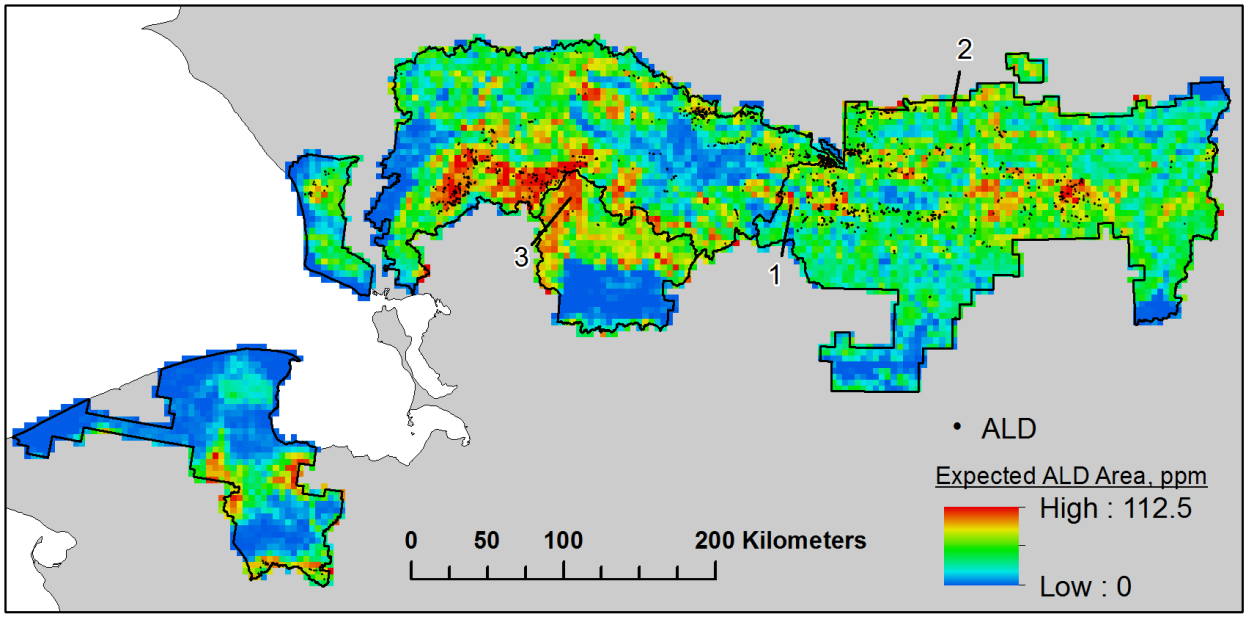

Figure 12. Expected ALD density in ARCN. The expected density of ALD (in proportion of area times 10^6, i.e. ppm area) was based on the observed relationship between ALD and slope steepness, with areas of unsuitable ecotypes masked (see the Methods section for details). Dots mark observed ALD locations. Numbers refer to areas with few ALD, discussed in the text.

There are some regions with apparently suitable terrain where ALD are lacking, such as central BELA, northern KOVA, and scattered areas in NOAT and GAAR (Fig. 12). Examination of the imagery these areas in some cases failed to reveal obvious factors that would prevent ALD formation, but in other areas there were features that provided clues as to why ALD were not present. For example, in area 1 of Fig. 12, southwest of the Noatak River in western GAAR, there are several RTS that appear to have developed from ALD, and hence this is not a true "blank spot" in ALD occurrence. Area 2 in Fig. 12 (east of the Killik River in northern GAAR) contains numerous revegetated ALD (Fig. 13), suggesting that the most susceptible areas had released in a previous event. Area 3 in northern KOVA is a unique part of ARCN with rather dense stands of tall shrubs on slopes above forested river valleys; spring snow persists later here than in areas at similar elevation to the northeast (Macander and Swingley 2012), probably as a result of deeper winter snowpacks. While tall shrub vegetation and deep snow themselves do not preclude ALD formation, they may be linked to soil conditions that are less favorable to ice segregation (e.g., warmer soil temperatures or coarser grain size) and thus less prone to ALD formation.

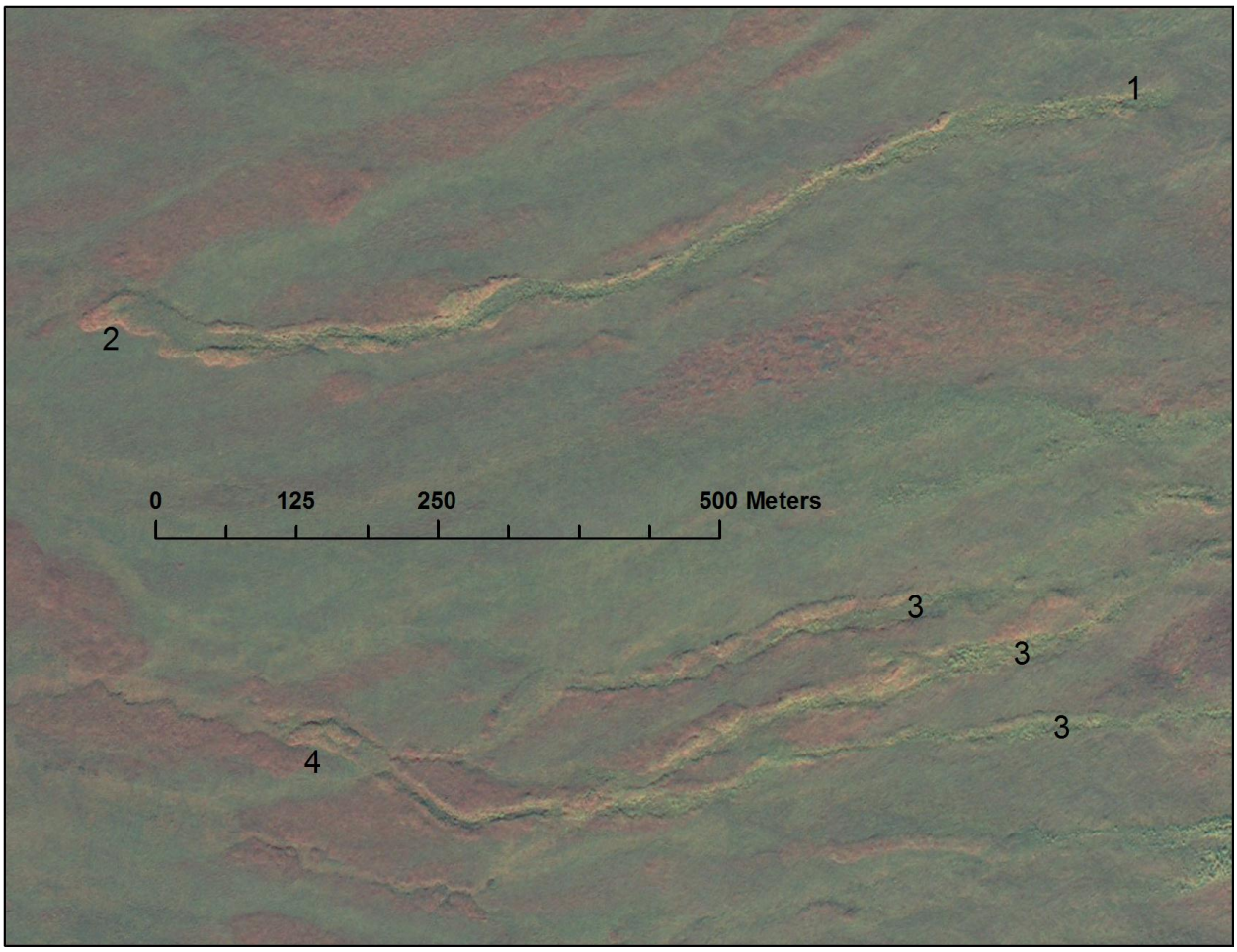

Figure 13. Revegetated former ALD in the Killik River valley of northern GAAR (near point 2 in Fig. 12; longitude -153.98°, latitude 68.32°). A large ALD, revegetated on this August 2006 IKONOS image, originated near point 1 and extended to point 2. Another complex ALD originated near multiple points labeled "3" and ended near point 4. These features are visible and completely vegetated on color infrared aerial photographs taken in August of 1982 as well as this 2006 image.

Time of ALD Events

Revegetation of recent ALD was apparent after two years, based on observations in the few places where overlapping satellite images from different dates were available (Fig. 14). My informal observations of ALD in NOAT and GAAR in 2010-13 gave me the distinct impression that new ALD had not formed in those years and existing ALD were revegetating, except where erosion continued by running water or by retrogressive thaw slumping (see below).

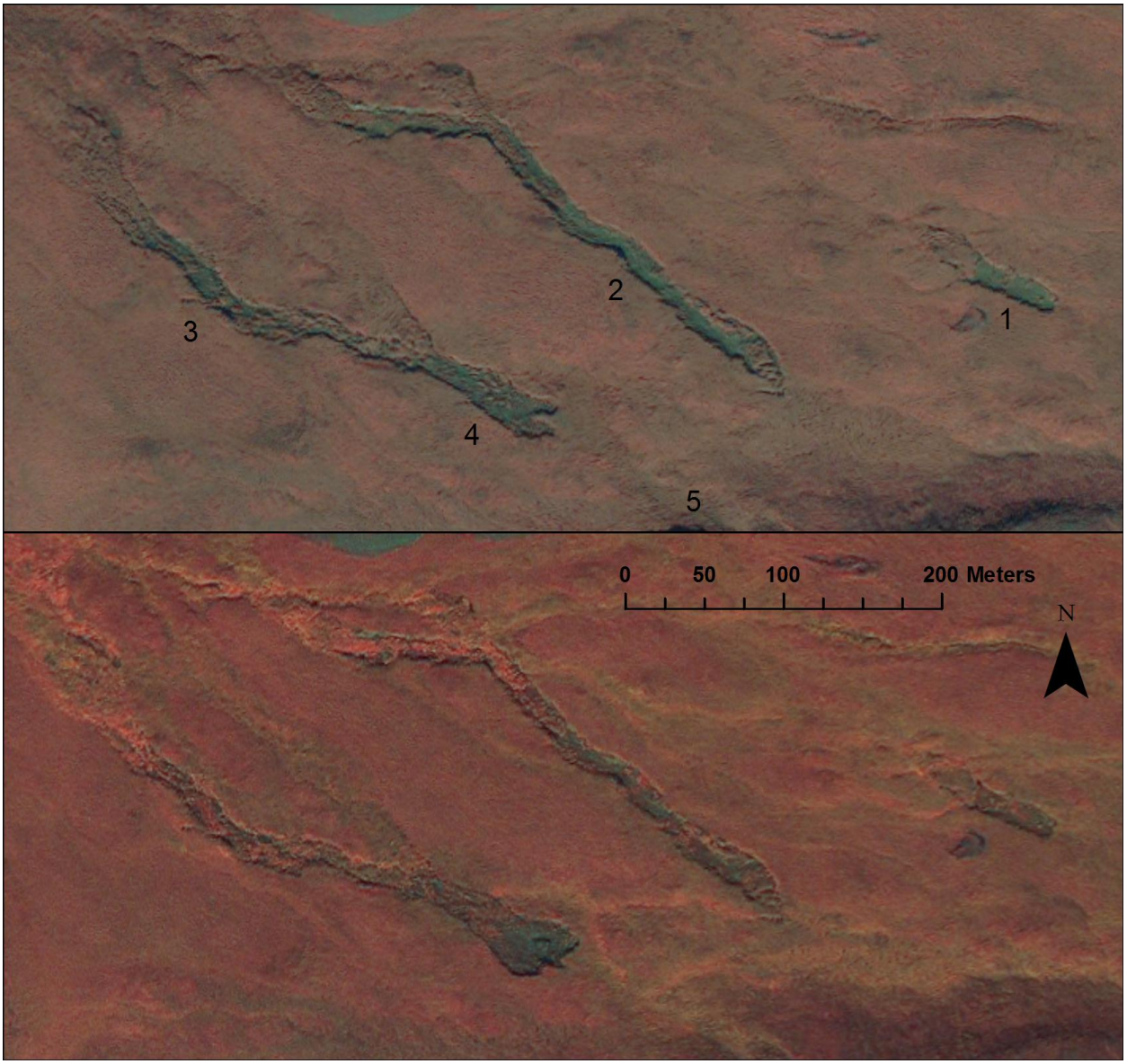

Figure 14. Revegetation of ALD between 2006 and 2008. The upper image (IKONOS image, 9 Sept 2006) shows 3 fairly fresh ALD. Gray is bare soil and reddish areas are green vegetation. The lower image (IKONOS image 15 Aug 2008) shows nearly complete revegetation of detachments at (1), (2), and (3). At location (4) the ALD continued to expand as a RTS, maintaining an area of grayish bare soil. An aerial photograph of the area from July 1978 showed undisturbed ground in the locations of these three ALD, but an active RTS (now revegetated) was present at (5). Near longitude -157.98°, latitude 68.23° in northeastern NOAT.

ALD formation requires both suitable site conditions and a trigger event consisting of warm summer weather, possibly augmented by rainfall (Carter and Galloway, 1981; Lewkowicz and Harris, 2005). Weather data from the Noatak RAWS, located in the central part of NOAT, shows that the summers of 2004 and 2007 were exceptionally warm and could be responsible for the ALD mapped in this study (Fig. 15). The much longer record for Kotzebue shows that 2004 was the warmest in the entire period of record (1950-2013; Fig. 15). ALD require a period of "pre-conditioning" during which segregated ground ice accumulates in the upper permafrost (Lewkowicz and Harris, 2005). The

length of time required for pre-conditioning is unknown, but is likely to be decades to centuries. Slopes are more stable for a period of years after a major ALD event, because the most susceptible sites have thawed and slid. Thus if 2004 and 2007 were similar in rate and maximum depth of thaw, we would expect the former year to have produced more ALD. Areas of overlap between images from the different years (2006-2009) that were examined as a part of the mapping process showed essentially no changes in ALD during this period except for some revegetation (i..e no new ALD), suggesting that indeed the main event was in 2004 rather than 2007.

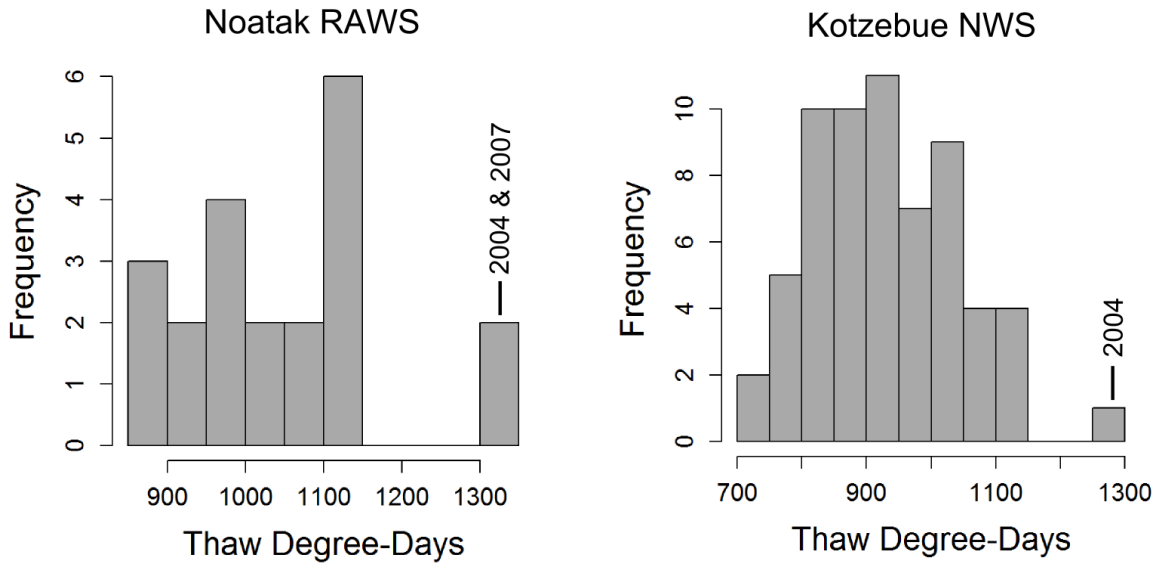

Figure 15. Thaw degree-days for the Noatak RAWS and Kotzebue NWS. Thaw degree-days (base temperature 0°C) for June, July, and August were computed using the full period of record (1992-2012 at Noatak RAWS, 1950-2012 at Kotzebue NWS). The years responsible for the outlier bars on the right (warm) side of the graph are identified.

Precipitation records for Kotzbeue NWS and Noatak RAWS in the period 2000-2006 did not reveal high precipitations events linked to warm summers that would suggest a precipitation trigger of ALD activity. At both stations the July-August total precipitation was near or below normal except years 2000, 2001, and 2003, but these summers had average or below-normal thaw degree-day totals. The year 2004 had near-normal precipitation at both stations.

The episodic nature of ALD and their revegetation within a matter of years presents problems for determining trends with time in ALD occurrence. Retrospective study of ALD frequency using historical imagery would be difficult in ARCN, because we have just two early image dates for most of our region (early 1950s and approximately 1980). Since the formation of ALD is episodic and infrequent, and revegetation makes them difficult to map after just 5 years or so, then we are likely to miss most ALD events if we have gaps of 30 years between samples. In addition, historical imagery generally has poorer resolution than the IKONOS imagery used here, and the 1950s imagery is panchromatic (black and white). ALD are visible on the c. 1980 color-infrared photography, but any difference in the number or area of ALD between then and today would be difficult to interpret

because of the lower detectability of ALD on the older photos. Future monitoring of ALD should be easier, if we are able to obtain high-resolution imagery soon after an ALD event identified by observers or suspected from weather records.

ALD Precursors of RTS

ALD often occurred in the vicinity of RTS, and in some cases it appears that the ALD produced the initial exposure that developed into an RTS (Figs 14 and 16.). One reason for a close association of ALD and RTS could be the presence of buried glacial ice. As will be discussed below, many of our RTS appear to be due to thaw of buried glacial ice masses. A deep summer thaw event that reaches buried glacial ice below the active layer could produce an ALD, as the active layer slides on a mud slurry over ice. Or, ALD could form due to thaw of segregated ice (as discussed above) in the sediment over the glacial ice, and the resulting scar would be highly susceptible to further development as a RTS, since the ALD removed the protective overburden of sediment on the buried glacial ice.

Figure 16. ALD precursors of RTS. At left is a vertical aerial photo by Tom George on 19 Aug 2008, on the right is an oblique aerial photo of the same area by Rory Nichols on 7 July 2013. Three partly revegetated ALD are visible above an active RTS on the left. The green line on the 2008 photo marks the upper end of the retrogressive thaw slump in that year, while the blue line shows its approximate extent in 2013, as shown by the photo on the right. The RTS appears to have started at the lower end of the three ALD, most likely soon after the widespread 2004 ALD event in ARCN. The Noatak River is visible in the foreground. The distance from the river to the steep scarp in the 2013 photo is about 300 m. Erosion feature NOAT265, longitude -161.09°, latitude 67.95°.

Ecological Implications of ALD

Soil erosion following ALD can deliver sediment and solutes to nearby streams (Lamoureaux and Lafrenière 2009, Bowden et al. 2008, 2012). The numerous ALD that formed in the mid-2000 decade were alarming to observers at the time (e.g., Balser et al. 2007). Indeed, if the level of ALD activity that was observed in 2004 were to become a frequent occurrence in a warming climate, this could cause significant environmental change, both through the effects of erosion on water quality and the increase in shrubby, early seral vegetation. In a warming climate, the activity of ALD that result from melting of segregated ice in the transient layer should eventually taper off as the ice supply on

suitable sites is exhausted, but we have no information about how much area might be affected before this happens.

Fortunately no other major ALD events have occurred in ARCN in the past 10 years since 2004. While we have no quantitative data on ALD revegetation, my informal observations discussed above suggest that the ALD that developed in 2004 have mostly revegetated. The narrow footprint of ALD and presence of vegetated islands within them ensures a nearby seed source for revegetation. The over 2000 ALD observed in this study are impressive, but the approximately 300 ha of bare soil exposed appears less significant, considering the huge area involved (82,000 km^2 in ARCN). For comparison, the area of riverine barrens (sand and gravel bars along rivers) in ARCN was estimated to be about 46,000 ha (Jorgenson et al. 2008), or about 150 times greater than the area in ALD; also, unlike some ALD, these riverine barrens are all in close contact with rivers and streams.

A more lasting legacy of the ALD mapped in this study may be the RTS that they set in motion. Even if most ALD revegetate within a few years, those that transform into RTS can last much longer and have much greater impacts (e.g. Fig. 16).

Retrogressive Thaw Slumps

RTS Overview

A total of 724 RTS were identified in ARCN, nearly all of them in NOAT and GAAR (Table 1, Fig. 17). The total area of bare soil mapped in RTS was about 235 ha. The largest feature, which appeared to be a result of both retrogressive thaw slumping and active layer detachments, covered approximately 9 ha in northwestern GAAR (Fig. 18). Aside from this exceptionally large feature, the largest RTS in ARCN were just over 4 ha (e.g., Fig. 19), and size ranged down to a few tens of square meters in small or nearly revegetated features. The vast majority of RTS in ARCN were in the Noatak River watershed in NOAT and GAAR, though the small Nigu-Etivluk watershed (northeastern NOAT and northwestern GAAR) had a much higher concentration of RTS per unit area (Table 2).

No RTS were found in BELA or CAKR, and the 3 small features identified in KOVA were poor examples of RTS that in fact are somewhat doubtful but were included for thoroughness and to mark them for future observations.

RTS and Environmental Factors

The median slope of RTS as measured by GIS analysis was 16%; the mean was 17%. Two-thirds of all pixels in RTS had slopes between 7% and 25%; 80% were between 4% and 30% slope, 90% were between 2% and 34% slope (Fig. 10). RTS were most common on northwest-facing slopes and least common on south- and southeast-facing slopes (Fig. 20).

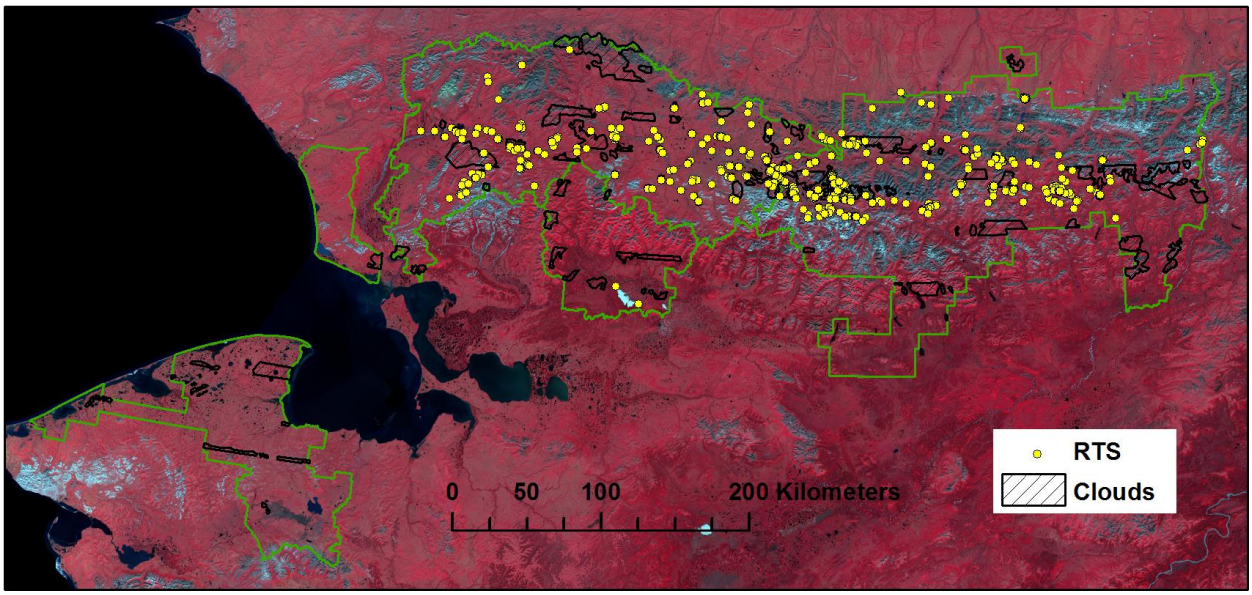

Figure 17. Retrogressive thaw slumps (RTS) in ARCN. Areas outlined as “clouds” were obscured on the imagery and mapping is incomplete.

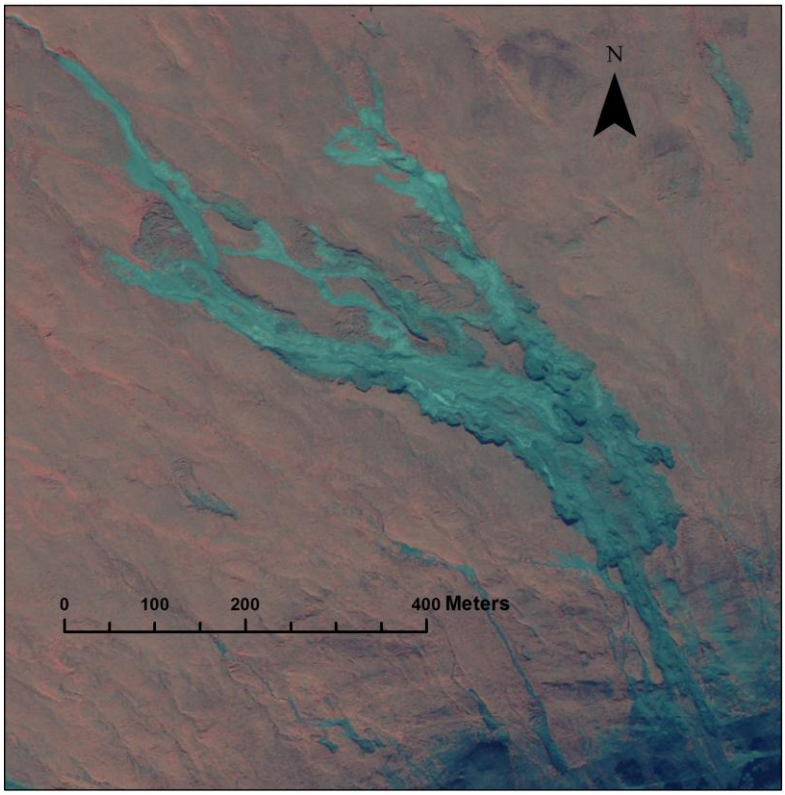

Figure 18. The largest RTS mapped in ARCN covers about 9 ha in far northwestern GAAR near Siavlat Mountain (GAAR1793, longitude -155.49°, latitude 68.05°, IKONOS image 5 July 2007). Both retrogressive thaw slumping and active layer detachments were probably active here. Bedrock (the nearly black areas near the lower right edge of the photo) is exposed on the mountain to the south. A July 1979 aerial photograph of this area shows an undisturbed slope

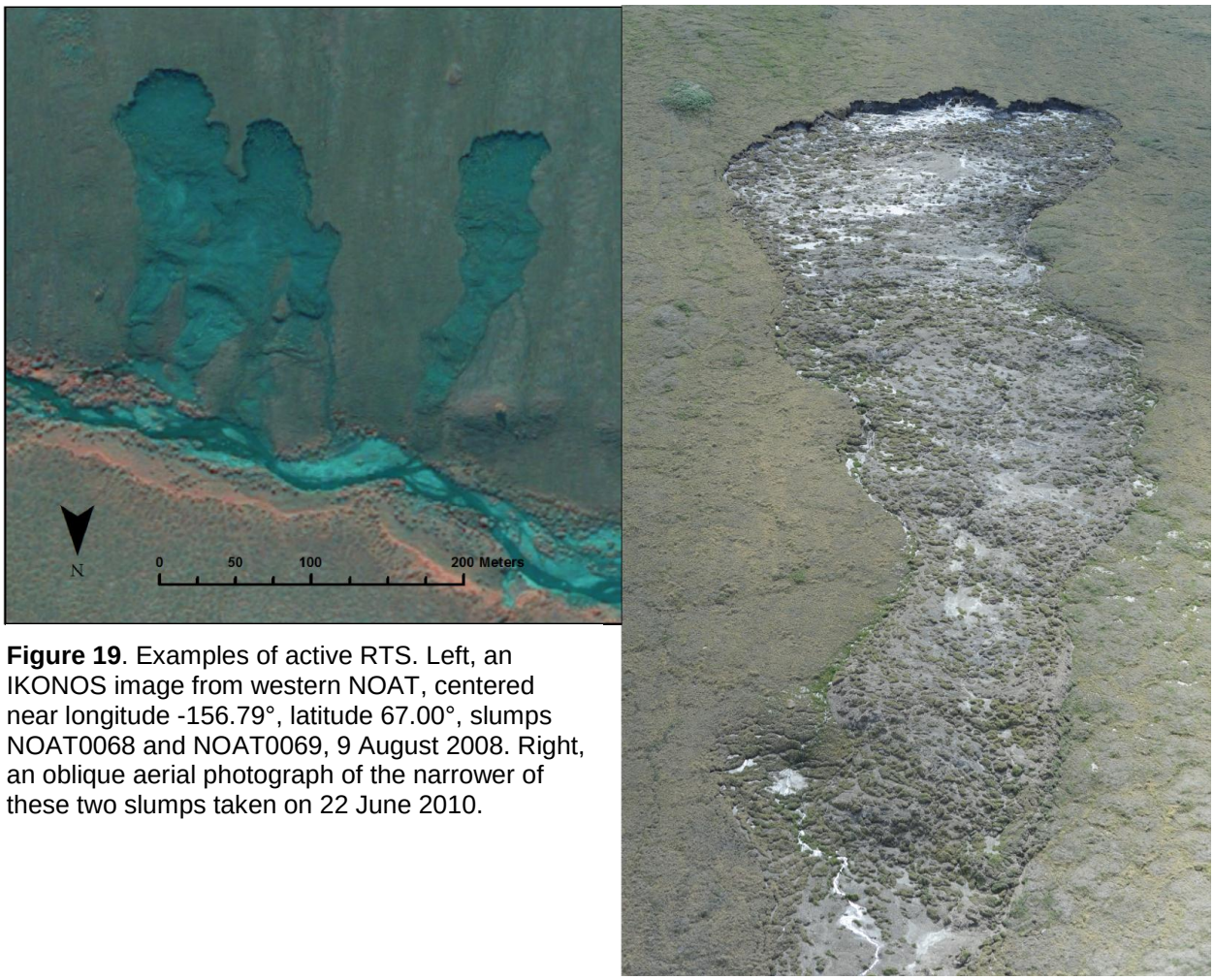

Figure 19. Examples of active RTS. Left, an IKONOS image from western NOAT, centered near longitude -156.79°, latitude 67.00°, slumps NOAT0068 and NOAT0069, 9 August 2008. Right, an oblique aerial photograph of the narrower of these two slumps taken on 22 June 2010.

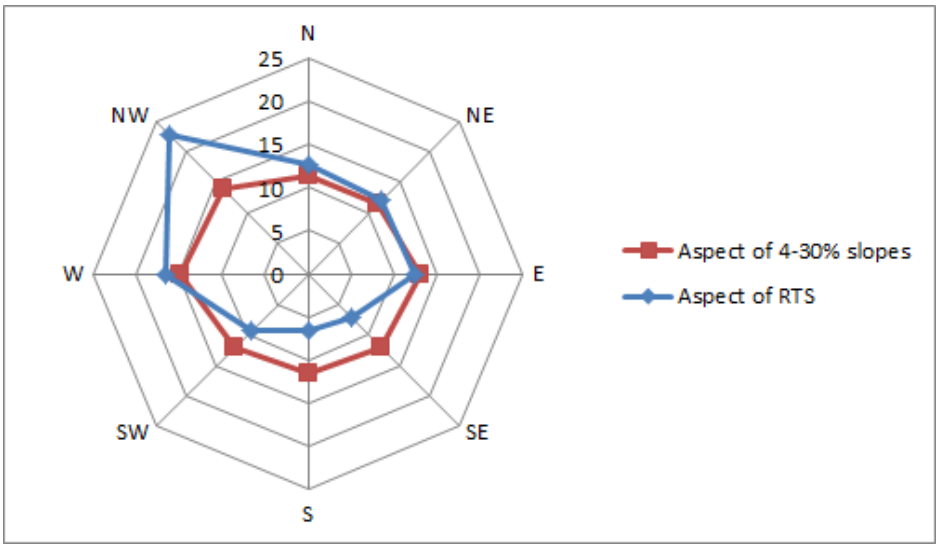

Figure 20. Slope aspects of RTS. ”Aspect of RTS” is the percentage of all bare-soil pixels in RTS with the indicated aspect. For example, about 23% of the RTS area had northwest aspects (between 292° and 238°). The red line is gives proportion of each aspect in ARCN on slopes with steepness in the optimal range for RTS (4 to 30%).

The fact that RTS occurred preferentially on northwest-facing slopes and are less common on south-facing slopes is perhaps counter-intuitive, as one might expect them to occur on warm slopes where ice is more likely to thaw. Perhaps the large ice bodies required for RTS (e.g., Pleistocene glacial ice, see below) have not been preserved on some south-facing aspects. These findings are consistent with Kokelj et al. (2009), who found RTS to be most common on north-facing slopes in northwestern Canada.

In ARCN the typical settings for RTS were:

- Along rivers or creeks (n = 241, 84.9 ha). A steep slope or bluff near the stream was the initiation point for the RTS and sediment from the RTS can move directly into the stream.
- Along lake shores (n = 97, 27.1 ha). A steep slope or bluff next to the lake was the initiation point for the RTS and sediment from the RTS can move directly into the lake.
- On upland slopes away from water bodies (n = 385, 123.4 ha). Sediment released by the RTS is deposited primarily on adjacent tundra.

The surficial geologic settings of RTS were complex. The most common unit mapped at RTS locations in ARCN by Hamilton (2010) and Hamilton and Labay (2011) was "bedrock", i.e. slopes interpreted to have minimal mantle of surficial deposits. RTS can only develop in unconsolidated material, and closer examination reveals these RTS were actually in patches of unconsolidated deposits that occur in a mosaic on the landscape with bedrock knobs and ridges and are joined with the latter at the scale of Hamilton's mapping (1:300,000). Most RTS mapped on surficial deposits were on glacial deposits from various phases of the late-Pleistocene Itkillik glaciation.

Examination of exposures of sediment and ground ice in 13 RTS in NOAT by Swanson and Hill (2010) and Swanson (2012a) showed them to be exclusively in glacial till deposits, and glacial ice was present under a surface layer of glacial till in many main scarp exposures (Fig. 4). The identification of glacial ice in permafrost is controversial; Mackay and Dallimore (1992) disputed the glacial origin of massive ground ice in glacial tills of northwestern Canada, and scientists there have searched for non-glacial explanations for the ice causing RTS in these tills (Lacelle et al., 2004). However, more recent work in northwestern Canada by Murton et al. (2005) has supported a glacial origin for massive tabular ice bodies under till, similar to what we observed in NOAT. Kanevskiy et al. (2008, 2013) identified probable glacial ice in a coastal exposure in northeastern Alaska.

Glacial till deposits are widespread in NOAT and GAAR (Hamilton 2010, Hamilton and Labay 2011) and, owing to their location in the continuous permafrost zone, these tills may conceal relict glacial ice in many places. Most of NOAT and GAAR were glaciated in the late Pleistocene, so relict glacial ice is potentially present nearly anywhere that glacial till indicates the former ice extent and could protect the ice from thaw. The glacial tills observed in RTS exposures by Swanson and Hill (2010) and Swanson (2012a) were relatively fine-grained, which makes them susceptible to liquefaction by super-saturation with water when the underlying ice melts. These tills probably originated mainly from subglacial material (potentially including older till, colluvium, alluvium,

loess, and lacustrine sediment) that were entrained into basal glacial ice and then mixed upward by deformation (Hubbard et al. 2009). Partial ablation of the ice eventually brought these basal sediments on top of the remaining ice. If the glacial ice contained enough debris to allow a meter or two of dominantly fine-grained sediment to accumulate on the surface through ablation before exhausting all of the ice, the supraglacial debris layer would be thicker than typical active layers in fine-grained sediments of this region, and any remaining glacial ice would be preserved in permafrost.

No true RTS were identified in the very ice-rich yedoma terrain of northern BELA. Thermokarst processes are ubiquitous there; lake shore bluffs are often over 10 m high with the characteristic mounds that develop when ice wedges disintegrate (Fig. 21). Unlike RTS, these escarpments have not advanced away from their original position near the water's edge. In spite of the high ice content of yedoma sediments, these thawing slopes stabilize at a rather steep angle and the escarpment has its base at the water's edge. Possible reasons for the relative stability of these slopes includes the horizontally discontinuous nature of wedge ice, and the generally flat slope of the surfaces between the lakes. Both characterstics probably limit transport of sediment away from the thawing escarpment, allowing sediment to build up and protect the permafrost.

Figure 21. Lakeshores in yedoma terrain of northern BELA. The lake in the foreground is about 500 m long and the bluffs at their highest points are about 25 m above these lakes. The numerous small mounds on the bluff slopes, especially visible on the slope on the left side of the nearer lake, are the centers of ice-wedge polygons that have disintegrated. In spite of the very ice-rich material, these escarpments have *not* migrated away from the lake to form retrogressive thaw slumps. Longitude -164.625°, latitude 66.292°.

Fine-grained lacustrine deposits or glacial tills could contain enough ground ice of non-glacial origin (e.g., ice wedges and segregated ice) to produce RTS where adequate slope is present, but the sloping morainal terrain with continuous tabular bodies of buried glacial ice are clearly ideal for RTS formation.

The vegetation in the vicinity of RTS was similar to ALD and included all of the widespread upland tundra types (Table 4). Lacking were barrens ecotypes and all coastal, lowland, riverine, and forested ecotypes.

Table 4. Vegetation Near Retrogressive Thaw Slumps.

Ecotype[1]	Percentage of RTS area in ecotype[2]	Percentage of ARCN occupied by ecotype
Alpine Dryas Dwarf Shrub	20.2	14.3
Upland Dwarf Birch-Tussock Shrub	20.0	20.1
Upland Birch-Ericaceous-Willow Low Shrub	15.9	11.3
Upland Sedge-Dryas Meadow	12.8	6.0
Upland Alder-Willow Tall Shrub	5.0	4.9

[1]Ecotypes are composite soil-vegetation units mapped by classification of 2002 Landsat satellite imagery by Jorgenson et al. (2008).

[2]These proportions reflect vegetation in and within a few tens of meters of the mapped RTS outlines (as a result of the 30 m resolution of the ecotype map), prior to their formation (because most were much smaller or not present in 2002). The table includes all types that occupy 5% or more of the total RTS area; together these 5 ecotypes account for 74% of the area in ALD.

RTS Susceptibility

The ice bodies responsible for RTS cannot be observed directly, and surface manifestations of their formation (analogous to ice-wedge polygons as indicators of wedge ice) are lacking. Our available GIS layers of slope, aspect, vegetation can be used to eliminate obvious unsuitable areas, but such an analysis would simply identify the extensive areas of gently sloping tundra where RTS are only locally present. Unfortunately, as discussed above, the available surficial geology map units did not differentiate well between areas of RTS and areas without.

The best predictor of RTS at the present time is other active or revegetated RTS that indicate the presence of large ground ice bodies. RTS can pass repeatedly across the surface of the same buried ice mass, stripping a layer of ice away and then stabilizing before the ice is exhausted (Lantuit and Pollard 2008, Kokelj et al. 2009; see also slump NOAT151 in Swanson and Hill 2010 and Swanson 2012a, 2013). A map of the current density of RTS in ARCN is presented in Fig. 22. Future monitoring efforts could be targeted to these areas of know susceptibility to reduce cost.

RTS Timing

Revegetated RTS were frequently visible in the vicinity of active RTS (e.g., Fig. 3). One dense aggregation of revegetated RTS in northwestern GAAR had no active features, and examination of historical aerial photos show that slumps there were most active in the 1950s (Fig. 23). This was the only case of multiple revegetated RTS observed without an active RTS nearby.

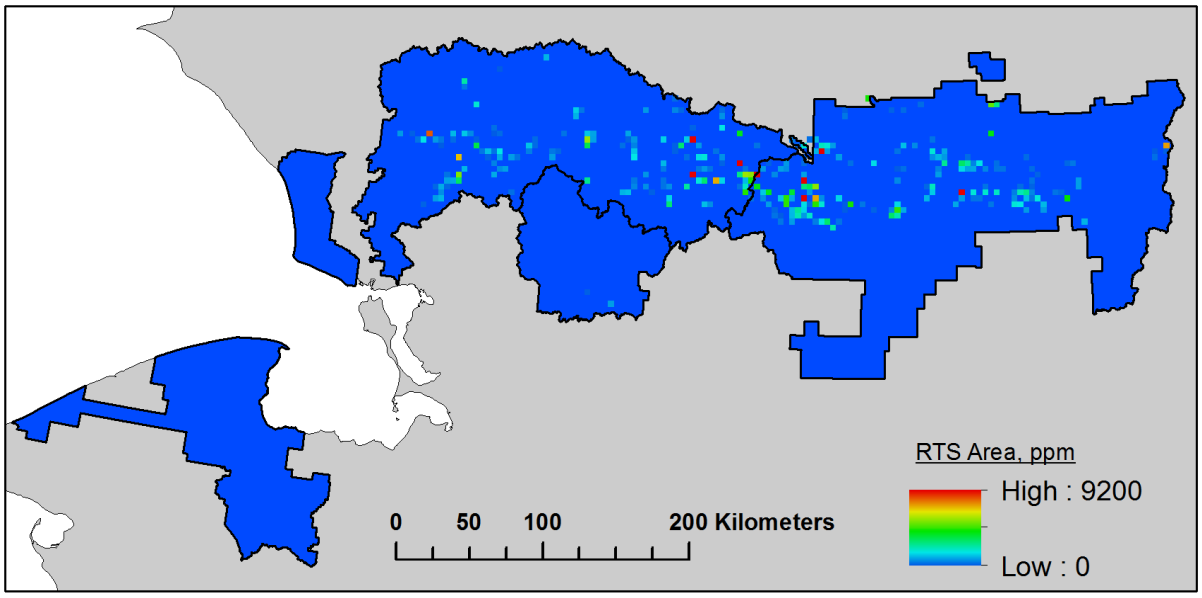

Figure 22. RTS density in ARCN. The mapped area of bare soil in RTS was summed for 4 km by 4 km pixels and expressed in units of % area times 10^4, equivalent to the proportion of area times 10^6 (ppm).

Monitoring of selected RTS in NOAT and GAAR by Swanson (2013) suggests that many of the active features we see today were initiated in the late 1990s and early 2000s. Some RTS have ceased expansion or nearly so, while others continue to grow rapidly, with escarpment retreat rates as high as 30 m y^{-1}. Thus individual RTS can enlarge for a decade or two in one spot and then stabilize (Figs. 23 and 24). RTS can also go through multiple periods of activity and quiescence for many decades in the same area (Fig. 25; Liposvsky and Huscroft 2006).

Because they are long-lived, a retroactive study using historical imagery can be used to determine if RTS are more or less widespread today than in the past. Studies of RTS in northwestern Canada using historical imagery by Lantuit and Pollard (2008) and Lantz and Kokelj (2008) showed an increase in rate of RTS growth in the 1970s, 80s and 90s relative to the 1950s and 60s. A 190 km^2 portion of my study area in NOAT had more and larger slumps on 2008 IKONOS imagery than aerial photos from 1977 (Swanson 2012b).

Mapping of RTS on both historical aerial photographs and future imagery would be useful to establish trends in RTS activity in ARCN. My trial mapping of RTS on historical aerial photos mentioned above (Swanson 2012b) indicated that 1980s-era color-infrared aerial photographs (which are available for all of ARCN) are suitable for mapping RTS by the same method as was used here; however, their effective resolution appears to be a little lower than our 1-m IKONOS images, and such a study would require high-resolution scanning (1000 dpi or better) and orthorectification, or at least careful georeferencing. Earlier (c. 1950) panchromatic (black and white) aerial photos of ARCN are suitable for visual comparisons such as Figs. 23 and 24 and manual mapping of some RTS, but it would be difficult to distinguish true temporal trends in RTS area from false trends due to the difficulty in identifying RTS on the 1950s-era photos. Fortunately, for future mapping we can hope to acquire data from satellite sensors with characteristics similar to or better than the IKONOS images used in the present study, and the mapping method used here could be repeated.

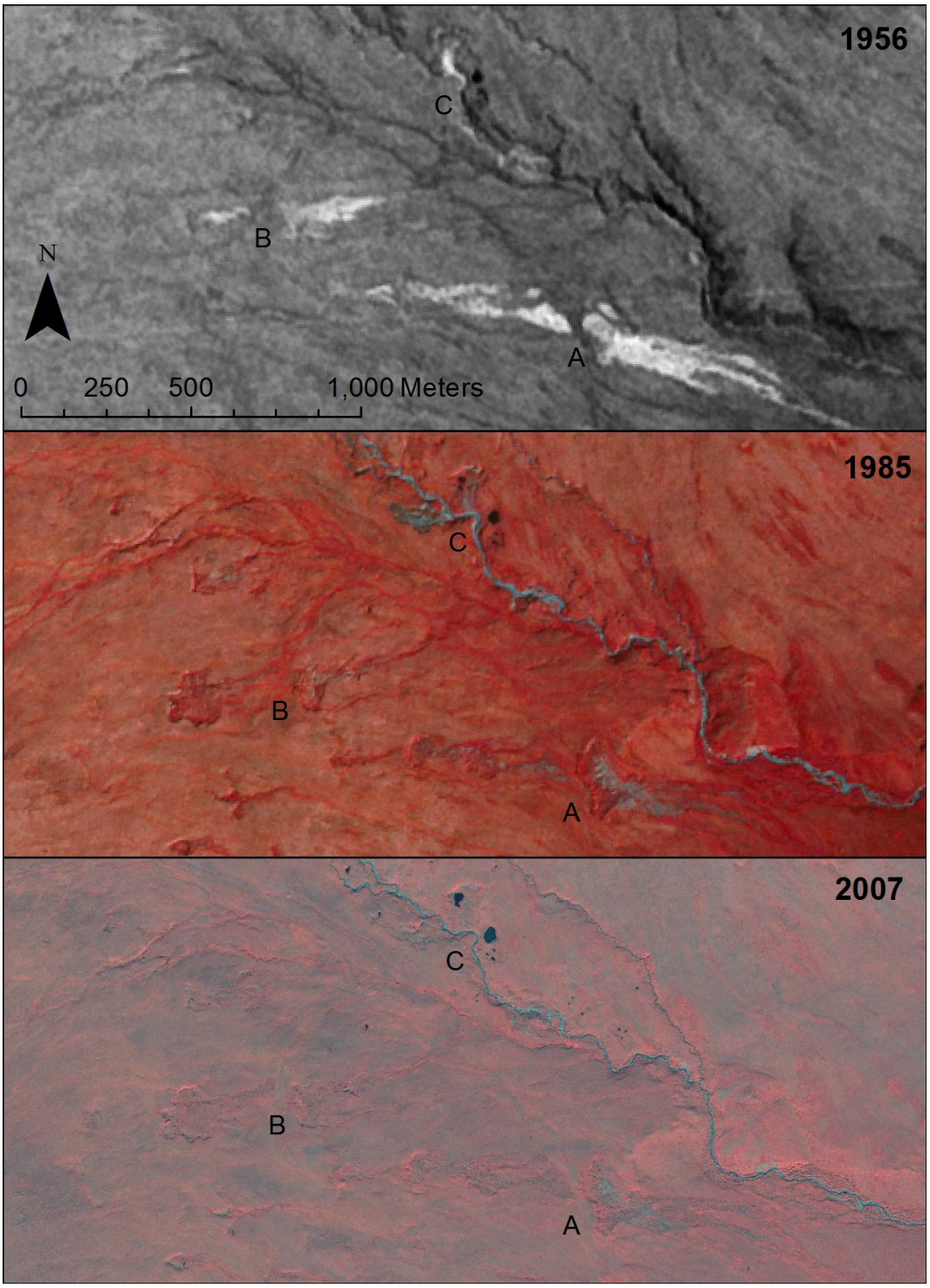

Figure 23. Revegetated RTS near the Killik River in northeastern GAAR. The July 2007 IKONOS satellite image shows multiple old slumps. The slumps near “A” were active in 1956 (GS-TAL, 7-11-56, frame 35-65-L), and revegetated with little additional growth by 1985 (AHAP 03476 19-AUG-85 frame 9057). The slumps near “B” were active in 1956; the one above and to the left of “B” enlarged after 1956 before stabilizing by 1985. The slump above “C” was active in 1956 and changed little thereafter, although enlarging ponds suggest continued subsidence. The slump above and to the left of “C” was not present in 1956, but was active in 1985, and grew little thereafter before stabilizing.

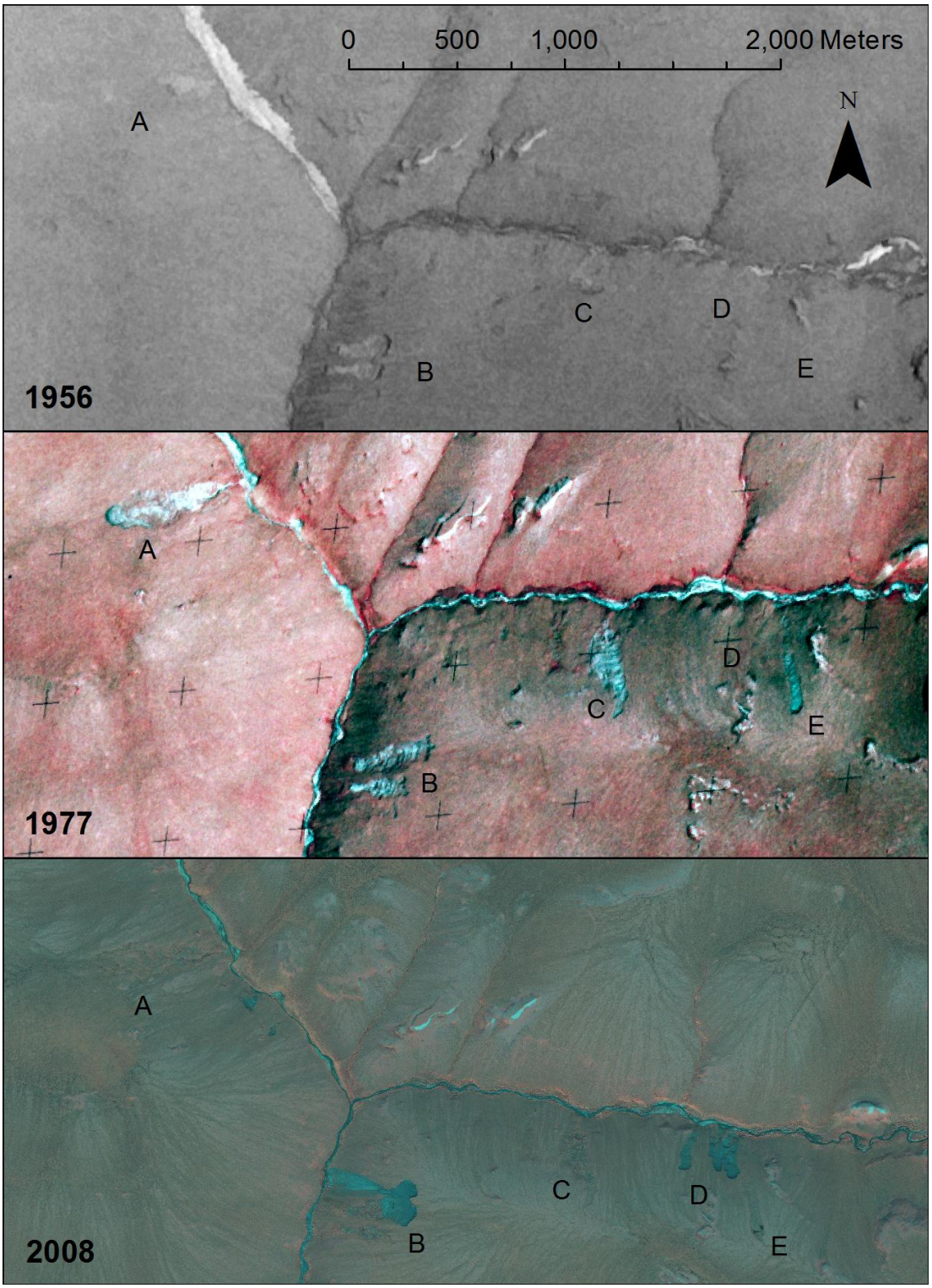

Figure 24. RTS activity in 1956, 1977, and 2008 in the upper Noatak valley. The slumps at A and C were active in 1956, larger and still active in 1977, and completely revegetated in 2008. The two slumps at B were active in 1956, larger and apparently stabilized in 1977, and revegetated in 2008; a large new slump was present in 2008 that partly overlapped the earlier ones. The slumps at D were not present in 1956 or 1977 but very active in 2008 (see also Fig. 20). The slump at E was absent in 1956, active in 1977, advanced about 100 m and stabilized by 2008. Longitude -156.82°, latitude 67.96°

Analysis of sufficient historical imagery to determine if an ARCN-wide trend is underway was not undertaken here due to time constraints. It would take a large study area – preferably most of the areas susceptible to RTS shown in Fig. 22 – to determine if a regional change driven by climate change is underway, because RTS activity has not been strongly synchronous over large areas. For example, the area in GAAR depicted in Fig. 23 was more active in 1956 than in 1985 and completely inactive in 2007, while an excerpt from the NOAT study area of Swanson (2012b) (Fig. 24) with imagery from 1956, 1977, and 2008 had active slumps with considerable exposed bare soil in all three years.

RTS Revegetation and Impacts

Bowden et al. (2012) found that 40-year-old RTS had revegetated, and their soil carbon and nitrogen stocks had recovered to resemble nearby undisturbed areas. Bartleman et al. (2001) documented the rapid revegetation of an RTS in the Yukon Territory, Canada, with shrub cover well established after 10 years and young forest after 25 years. Informal observations made as a part of RTS monitoring in ARCN (Swanson and Hill 2010, Swanson 2012a, 2013) confirm the rapid revegetation of RTS; revegetation is enhanced by propagules from the ubiquitous small islands of vegetation present on the floors of RTS, which originate from blocks of turf that fell down main scarp. However, continued sedimentation from growth of the slump can prevent revegetation. Also, we have observed cases where vegetation remained sparse on RTS for decades after stabilization (e.g. slump GAAR008 in Swanson and Hill 2010), typically where good drainage allows silt-rich sediments to compact into a hard, dry surface.

The examples in Figs. 23 and 24 illustrate that revegetation in a few decades does not indicate return to pre-slump conditions, as obvious vegetation differences persist in old slump scars for at least 50 years. From this perspective, slumps have effects similar to wildfire and man-made disturbances that disrupt the surface organic mat and promote seral vegetation adapted to warmer and less organic soils (certain herbs and deciduous shrubs) at the expense of evergreen shrubs, lichens, and certain mosses (Fig. 25; Bartleman et al. 2001).

Figure 25. Revegetation of a RTS. The moist bare sediment on the floor of this RTS was rapidly colonized by herbaceous seral species as the main scarp retreated. The large forb visible here is Mastadon flower (*Senecio congestus*). Slump NOAT0039 on 24 June 2010, longitude -159.291, latitude 68.036.

RTS have obvious impacts on water quality and stream characteristics, especially when they occur immediately on a stream or lake shore (Kokelj et al. 2005, Liposvsky and Huscroft 2006, Crosby 2009, Bowden et al. 2012, Barnhart and Crosby 2013). As in the case of ALD, the total area covered by RTS in ARCN (235 ha) is not large when compared to the huge land area involved (82,000 km^2 in ARCN) and the area of riverine barrens (46,000 ha, approximately 200 times greater than the area of RTS). Furthermore, as described above, over half of the RTS were on upland slopes distant from water bodies. At present levels of RTS activity, the most serious impacts of RTS are local and result from an individual large and active RTS near a water body. For example, the large RTS on the Selawik River in Selawik National Wildlife Refuge threatens a spawning area of sheefish (*Stenodus leucichthys*) with siltation (Hander et al. 2008, USFWS 2013). No similar threats of RTS to fish spawning habitat have been noted in ARCN, but they remain a possibility.

Modeling of future permafrost conditions in Alaska under warming scenarios generated by global circulation models out to the year 2100 (Marchenko et al. 2008) predict that the parts NOAT and GAAR where our RTS occur will generally retain permafrost, but with warmer mean annual ground temperatures (in the -0.5° C to -2.5° C range, i.e. typical of the discontinuous permafrost zone) and active layer thicknesses will be approximately double what they are today. RTS activity would increase dramatically under this scenario, as the thickened active layer encountered ground ice and permafrost was destabilized entirely from warm sites the landscape. The latter possibility is particularly alarming, because RTS activity on buried glacial ice would no longer be episodic, but instead would continue until the ice body involved is melted entirely.

Conclusions

Active-layer detachments (ALD) were common on 2006-2009 satellite images of ARCN; over 2000 were mapped. They were most abundant in the Killik, Noatak, and Nigu-Etivluk watersheds of NOAT and GAAR. They occurred on moderately steep (8-39%) tundra slopes with unconsolidated sediments. They were most common on northwest-facing slopes.

Most ALD revegetate in a few years after they form, and they appear to be particularly abundant on our images (2006-2009) as a result of an ALD-formation event just prior to the image dates (probably in 2004).

The environmental effects of ALD in ARCN were limited by the relative small area affected (a total area of 300 ha of bare soil from ALD in ARCN), their rapid revegetation in most cases, and the lack of major ALD events in the 10 years since 2004. However, the potential exists for ALD to cause important changes to water quality and local vegetation if events like the one in 2004 become more intense or more frequent.

Future monitoring of ALD should be at closely spaced time intervals (e.g., 5 years) or be triggered by field observations or weather records that suggest another event has occurred. Because slopes can be stabilized by an ALD event, future monitoring (if it is a sample rather than a comprehensive survey) should target both areas where ALD were abundant in the current survey (i.e. known slide-susceptible areas) and other areas with generally suitable conditions (slopes of 8-40% and tundra vegetation). Also, any wildfire areas on forested slopes should be examined for ALD within a few years of the fire. Available historical imagery is not well suited for a retrospective study of ALD occurrence in ARCN.

Retrogressive thaw slumps were also common on 2006-2009 satellite images of ARCN, with over 700 mapped. They were most abundant in the Noatak and Nigu-Etivluk watersheds of NOAT and GAAR. They occurred on glacial sediments with gentle to moderate slopes (4-30%) and tundra vegetation.

The environmental impacts of RTS, like ALD, are limited by the relatively small area involved (about 235 ha in all of ARCN) and the fact that the majority of RTS are distant from water bodies. Impacts to aquatic resources could be locally significant if a large slump develops near a sensitive location, such as a fish spawning area. Impacts could increase greatly if RTS become more abundant as a result of climate change.

The presence of RTS on historical aerial photographs from c. 1950 and c. 1980 shows that these features are not new to the study area. The abundance of these features on our 2006-2009 imagery could represent an increasing a trend resulting from recent climate change, but proof of this idea would require analysis of historical aerial photographs. RTS could be mapped on c. 1980 color-infrared aerial photographs of ARCN by similar methods to those used here, though a large area (i.e. significant effort) would be required to determine whether a change has occurred from 1980 to the

present, and differences in image quality between the c 1980 photos and today's high-resolution satellite images could make results inconclusive.

RTS are long-lived features that are readily monitored by regularly repeated surveys. Because individual RTS can grow for a decade or more, surveys repeated at an interval of 5 to 10 years seem appropriate to capture trends. To reduce cost and effort, future surveys (or retroactive surveys using historical imagery) could be targeted to areas known from this study to be susceptible to RTS. The susceptibility of a site to RTS is largely dependent on the presence of large ground ice bodies that have no surface expression except for scars from previous RTS. Hence the present distribution of active and stabilized RTS is currently our best predictor of future RTS locations.

Literature Cited

Balser, A. W. W. B. Bowden, J. B. Jones, M. N. Gooseff, D. M. Sanzone, A. Bouchier, and A. Allen. 2007. Thermokarst distribution in the Noatak Basin, Alaska: increased frequency and correlations with local and regional landscape variables. American Geophysical Union, Fall Meeting 2007, abstract #C32A-08.

Balser, A., J. B. Jones, and T. Jorgenson. 2010. Thermokarst associations with landscape characteristics in arctic Alaska: implications for future permafrost degradation at landscape to regional scales. American Geophysical Union, Fall Meeting 2010, abstract #C31A-0501.

Barnhart, T. B. and B. T. Crosby. 2013. Comparing two methods of surface change detection on an evolving thermokarst using high-temporal-frequency terrestrial laser scanning, Selawik River, Alaska. Remote Sensing 5:2813-2837; doi:10.3390/rs5062813.

Bartleman, A-P., K. Miyanishi, C. R. Burn, and M. M. Côté. 2001. Development of vegetation communities in a retrogressive thaw slump near Mayo, Yukon Territory: a 10-year assessment. Arctic 54(2):149-156.

Boggs, K. and J. Michaelson. 2001. Ecological subsections of Gates of the Arctic National Park and Preserve. National Park Service, Alaska Region, Anchorage, Alaska. Available from https://irma.nps.gov/App/Reference/Profile/ 664200(accessed 9 December 2013).

Bowden, S. B., M. N. Gooseff, A. Balser, A. Green, B. J. Peterson, and J. Bradford. 2008. Sediment and nutrient delivery from thermokarst features in the foothills of the North Slope, Alaska: Potential impact on headwater stream ecosystems. Journal of Geophysical Research 113, G02026, doi:10.1029/2007JG000470,2008.

Bowden, W.B., J.R. Larouche, A.R. Pearce, B.T. Crosby, K. Krieger, M.B. Flinn, J. Kampman, M.N. Gooseff, S.E. Godsey, J.B. Jones, B.W. Abbott, M.T. Jorgenson, G.W. Kling, M. Mack, E.A.G. Schuur, A.F. Baron, and E.B. Rastetter. 2012. An integrated assessment of the influences of upland thermal-erosional features on landscape structure and function in the foothills of the Brooks Range, Alaska. Tenth International Conference on Permafrost. Tyumen, Russia, Pechatnik Press:61-66.

Burn, C. R., and A. G. Lewkowicz. 1990. Retrogressive thaw slumps. Canadian landform examples – 17. The Canadian Geographer 34(3):273–276.

Carter, L. D., and J. P. Galloway. 1981. Earth flows along Henry Creek, Northern Alaska. Arctic, 34, 325-328.

Cheng, G. 1983. The mechanism of repeated-segregation for the formation of thick layered ground ice. Cold Regions Science and Technology 8:57-66.

Crosby, B. T. 2009. Progressive growth, modulated supply: How coupling and decoupling between an enormous retrogressive thaw slump and its depositional fan impacts sediment delivery to the

Selawik River, Northwest Alaska. American Geophysical Union, Fall Meeting 2009, Abstract U41C-0043.

Hamilton, T. D. 2010. Surficial geologic map of the Noatak National Preserve, Alaska. U.S Geological Survey Scientific Investigations Map 3036. Scale 1:300,000. Available from http://pubs.usgs.gov/sim/3036/ (accessed 9 December 2013)

Hamilton, T. D. and K. A. Labay. 2011. Surficial geological map of the Gates of the Arctic National Park and Preserve, Alaska. U.S. Geological Survey Scientific Investigations Map 3125. Scale 1:300,000. Available from http://pubs.usgs.gov/sim/3125/ (accessed 9 December 2013).

Hander, R. F., R. J. Brown and T. J. Underwood. 2008. Comparison of Inconnu Spawning Abundance Estimates in the Selawik River, 1995, 2004, and 2005, Selawik National Wildlife Refuge. Alaska Fisheries Technical Report Number 99, Fairbanks, Alaska. Available from http://www.fws.gov/alaska/fisheries/fish/Technical_Reports/t_2007_99.pdf (accessed 2 May 2014).

Hopkins, D. M.. 1963. Geology of the Imuruk Lake area, Seward Peninsula, Alaska. U.S. Geological Survey Bulletin 1141-C. U.S. Government Printing Office, Washington D.C.

Hubbard, B., S. Cook, and H. Coulson. 2009. Basal ice facies: a review and unifying approach. Quaternary Science Reviews 28:1956-1969.

Jorgenson, M. T. 2001. Ecological subsections of Bering Land Bridge National Preserve. Inventory and Monitoring Program, National Park Service, Alaska Region, Anchorage, Alaska. Available from https://irma.nps.gov/App/Reference/Profile/583322 (accessed 9 December 2013).

Jorgenson, M. T., Y. L. Shur, and E. R. Pullman. 2006. Abrupt increase in permafrost degradation in Alaska. Geophysical Research Letters 33:L02503.

Jorgenson, T., K. Yoshikawa, M. Kanevskiy, Y. Shur, V. Romanovsky, S. Marchenko, G. Grosse, J. Brown, and B. Jones. 2008. Permafrost characteristics of Alaska. Proceedings of the Ninth International Conference on Permafrost. University of Alaska Fairbanks, Institute of Northern Engineering. Scale 1:7,200,000.

Jorgenson, M. T., J. E. Roth, P. F. Miller, M. J. Macander, M. S. Duffy, A. F. Wells, G. V. Frost, and E. R. Pullman. 2009. An ecological land survey and landcover map of the Arctic Network. Natural Resource Technical Report NPS/ARCN/NRTR—2009/270. National Park Service, Fort Collins, Colorado.

Jorgenson, M. T., D. K. Swanson, and M. Macander. 2001. Landscape-level mapping of ecological units for the Noatak National Preserve, Alaska. Inventory and Monitoring Program, National Park Service, Alaska Region, Anchorage, Alaska. Available from https://irma.nps.gov/App/Reference/Profile/583328 (accessed 9 December 2013).

Kanevskiy, M., T. Jorgenson, Y. Shur, and M. Dillon. 2008. Buried glacial basal ice along the Beaufort Sea Coast, Northern Alaska. Eos Transactions, American Geophysical Union 89 (53) Fall Meet. Suppl., Abstract C11D-0531.

Kanevskiy, M., Y. Shur, D. Fortier, M. T. Jorgenson, and E. Stephani. 2011. Cryostratigraphy of late Pleistocene syngenetic permafrost (yedoma) in northern Alaska, Itkillik River exposure. Quaternary Research 75:584-596.

Kanevskiy, M., Y. Shur, M.T. Jorgenson, C.-L. Ping, G.J. Michaelson, D. Fortier, E. Stephani, M. Dillon, and V. Tumskoy. 2013. Ground ice in the upper permafrost of the Beaufort Sea coast of Alaska. Cold Regions Science and Technology 85:56–70

Kokelj, S. V., R. E. Jenkins, D. Milburn, C. R. Burn, and N. Snow. 2005. The influence of thermokarst disturbance on the water quality of small upland lakes, Mackenzie Delta region, Northwest Territories, Canada. Permafrost and Periglacial Processes 16:343-353.

Kokelj, S. V., T. C. Lantz, J. Kanigan, S. L. Smith, and R. Coutts. 2009. Origin and polycyclic behavior of tundra thaw slumps, Mackenzie Delta region, Northwest Territories, Canada. Permafrost and Periglacial Processes 20:173-184.

Lacelle, D., J. Bjornson, B. Lauriol, I. D. Clark, and Y. Troutet. 2004. Segregated-intrusive ice of subglacial meltwater origin in retrogressive thaw flow headwalls, Richardson Mountains, NWT, Canada. Quaternary Science Reviews 23(5-6):681-696.

Lacelle, D., J. Bjornson, and B. Lauriol. 2010. Climatic and geomorphic factors affecting contemporary (1950-2004) activity of retrogressive thaw slumps on the Aklavik Plateau, Richardson Mountains, NWT, Canada. Permafrost and Periglacial Processes 21:1–15.

Lamoureaux, S. F., and M. J. Lafrenière. 2009. Fluvial impact of extensive active layer detachments, Cape Boundary, Melville Island, Canada. Arctic, Antarctic, and Alpine Research 41(1):59–68.

Lantuit, H. and W. H., Pollard. 2008. Fifty years of coastal erosion and retrogressive thaw slump activity on Herschel Island, southern Beaufort Sea, Yukon Territory, Canada. Geomorphology 95:84–102

Lantz, T. C. and S. V. Kokelj. 2008. Increasing rates of retrogressive thaw slump activity in the Mackenzie Delta region, N.W.T., Canada. Geophysical Research Letters, Vol. 35, L06502, doi:10.1029/2007GL032433

Lawler, J. P., S. D. Miller, D. M. Sanzone, J. Ver Hoef, and S. B. Young. 2009. Arctic network vital signs monitoring plan. Natural Resource Report NPS/ARCN/NRR-2009/088. U.S. Department of the Interior, National Park Service, Natural Resource Stewardship and Science, Ft. Collins, Colorado.

Lewkowicz, A. G., and C. Harris. 2005. Frequency and magnitude of active-layer detachment failures in discontinuous and continuous permafrost, northern Canada. Permafrost and Periglacial Processes 16:115–130.

Lewkowicz, A. G. 2007. Dynamics of active-layer detachments failures, Fosheim Peninsula, Ellesmere Island, Nunavut, Canada. Permafrost and Periglacial Processes 18:89-103.

Lipovsky, P.S., J. Coates, A. G. Lewkowicz, and E. Trochim. 2006. Active-layer detachments following the summer 2004 forest fires near Dawson City, Yukon. Pages 175-194 *in* D. S. Emond, G. D. Bradshaw, L. L. Lewis and L. H. Weston, editors, Yukon exploration and geology 2005. Yukon Geological Survey, Whitehorse, Yukon Territory, Canada.

Lipovsky, P. and C. Huscroft. 2006. A reconnaissance inventory of permafrost-related landslides in the Pelly River watershed, central Yukon. Pages 181-196 *in* D .S. Emond, L. L. Lewis and L. H. Weston, editors, Yukon exploration and geology 2006. Yukon Geological Survey, Whitehorse, Yukon Territory, Canada.

Macander, M. J. and C. S. Swingley. 2012. Mapping snow persistence for the range of the Western Arctic Caribou Herd, northwest Alaska, using the Landsat archive (1985-2011). Natural Resource Technical Report NPS/ARCN/NRTR—2012/643. National Park Service, Fort Collins, Colorado.

Mackay, J. R., and S. R. Dallimore. 1992. Massive ice of the Tuktoyaktuk area, western Arctic coast, Canada. Canadian Journal of Earth Sciences 29(6):1235-1249.

Marchenko, S., V. Romanovsky, and G. Tipenko. 2009. Numerical Modeling of Spatial Permafrost Dynamics in Alaska. Pages 1125–1130 *in* D. L. Kane and K. M. Hinkel, editors, Proceedings of the Ninth International Conference on Permafrost. Institute of Northern Engineering, University of Alaska, Fairbanks.

Mayfield, C. F., I. L. Tailleur, and I. Ellersieck. 1988. Stratigraphy, structure, and palinspastic synthesis of the western Brooks Range, northwestern Alaska. Pages 143–186 *in* Geology and Exploration of the National Petroleum Reserve in Alaska. Professional Paper 1399. U.S. Geological Survey, Washington, DC.

Murton, J. B., C. A. Whiteman, R. I. Waller, W. H. Pollard, I. D. Clarke, and S. R. Dallimore. 2005. Basal ice facies and supraglacial melt-out till of the Laurentide Ice Sheet, Tuktoyaktuk Coastlands, western Arctic Canada. Quaternary Science Reviews 24:681-708.

Moore, T. E., W. K. Wallace, K. J. Bird, S. M. Karl, C. G. Mull, and J. T. Dillon. 1994. Geology of northern Alaska. Pages 49–140 *in* G. Plafker, and H. C. Berg, editors., The Geology of Alaska. The Geological Society of America, Denver, CO. The Geology of North America, Vol. G-1.

Péwé, T. L. 1975. Quaternary geology of Alaska. U.S., Geological Survey Professional Paper 835. U.S. Government Printing Office, Washington D.C.

Shur, Y., K. M. Hinkel, and F. E. Nelson. 2005. The transient layer: implications for geocryology and climate-change science. Permafrost and Periglacial Processes 16: 5–17.

Swanson, D. K. 2001a. Ecological subsections of Cape Krusenstern National Monument. Inventory and Monitoring Program, National Park Service, Alaska Region, Anchorage, Alaska. Available from https://irma.nps.gov/App/Reference/Profile/2197805 (accessed 9 December 2013).

Swanson, D. K. 2001b. Ecological subsections of Kobuk Valley National Park. Inventory and Monitoring Program, National Park Service, Alaska Region, Anchorage, Alaska. Available from https://irma.nps.gov/App/Reference/Profile/584437 (accessed 9 December 2013).

Swanson, D. K. 2010. Mapping of erosion features related to thaw of permafrost in Bering Land Bridge National Preserve, Cape Krusenstern National Monument, and Kobuk Valley National Park. Natural Resource Data Series NPS/ARCN/NRDS—2010/122. National Park Service, Fort Collins, Colorado.

Swanson, D. K. 2012a. Monitoring of retrogressive thaw slumps in the Arctic Network, 2011: Three-dimensional modeling of landform change. Natural Resource Data Series NPS/ARCN/NRDS—2012/247. National Park Service, Fort Collins, Colorado.

Swanson, D. K. 2012b. Mapping of erosion features related to thaw of permafrost in Noatak National Preserve. Natural Resource Data Series NPS/ARCN/NRDS—2012/248. National Park Service, Fort Collins, Colorado.

Swanson, D. K. 2013. Monitoring of retrogressive thaw slumps in the Arctic Network, 2012. Natural Resource Data Series NPS/ARCN/NRDS—2013/591. National Park Service, Fort Collins, Colorado.

Swanson, D. K., and K. Hill. 2010. Monitoring of retrogressive thaw slumps in the Arctic Network, 2010 baseline data: Three-dimensional modeling with small-format aerial photographs. Natural Resource Data Series NPS/ARCN/NRDS—2010/123. National Park Service, Fort Collins, Colorado.

Tucker C. J., and P. J. Sellers. 1986. Satellite remote sensing of primary production. International Journal of Remote Sensing 7(11):1395–1416.

US Fish and Wildlife Service [USFWS]. 2013. Selawik sheefish: murky future in a changing climate? Fairbanks Fish & Wildlife Field Office, Fairbanks, Alaska. Available from: http://www.fws.gov/uploadedFiles/Region_7/NWRS/Zone_2/Selawik/PDF/Selawik_Sheefish_2013.pdf (accessed 2 May 2014)

US Geological Survey [USGS]. 2006. National elevation dataset. Available from: http://ned.usgs.gov/ (accessed 19 Feb 2014).

USGS (U.S. Geological Survey). 2014. The National Hydrography Dataset. Available from http://nhd.usgs.gov/index.html (accessed 8 January 2014).

NPS 953/126782, October 2014

National Park Service
U.S. Department of the Interior

Natural Resource Stewardship and Science
1201 Oakridge Drive, Suite 150
Fort Collins, CO 80525

www.nature.nps.gov